CORROSION BEHAVIOUR OF IRON ALUMINIDES

by

MD. JAMIL AKHTAR

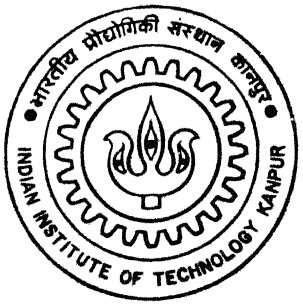

DEPARTMENT OF MATERIALS AND METALLURGICAL ENGINEERING

INDIAN INSTITUTE OF TECHNOLOGY KANPUR

JANUARY, 1995

CORROSION BEHAVIOUR OF IRON ALUMINIDES

A Thesis Submitted
in Partial Fulfillment of the Requirement
for the Degree of

MASTER OF TECHNOLOGY

by

MD. JAMIL AKHTAR

to the

DEPARTMENT OF MATERIALS AND METALLURGICAL ENGINEERING
INDIAN INSTITUTE OF TECHNOLOGY KANPUR

JANUARY 1995

MME-1995-M-AKH-COR

DEDICATED TO

My Parents

CERTIFICATE

It is certified that the work contained in the thesis entitled "Corrosion Behaviour of Iron Aluminides", by Md. Jamil Akhtar, has been carried out under my supervision and that this work has not been submitted elsewhere for a degree.

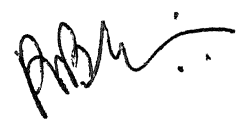

Dr. R. Balasubramaniam
Assistant Professor
Department of Materials and
Metallurgical Engineering
Indian Institute of Technology Kanpur

January 1995

ACKNOWLEDGEMENT

I Wish to express my heartfelt gratitude and sincere appreciation to *Dr. R.Balasubramaniam* for generous help,expert guidance and time,he provided in supervising this study, in spite of his very busy schedule. I am deeply indebted to him for imbibing in me the sense of joy of working towards a well defined goal.

I feel highly indebted to *Dr.M.N.Mungole* for extending full support during this work.

Special thanks are owed to *Mr.Rao* and *Mr.Gopinath* who helped me at different stages of work.

I am extremely thankful to *Arvind,Thakurji,Vidya,Shailesh* and all other friends whose names could not be listed, for reaching out their hands at crucial time.

M.J.Akhtar

ABSTRACT

Potentiodynamic polarization experiments were performed in electrolytes of pH 1.4, 4, 8 and 12 on stainless steels 304, 310, 316 and iron aluminide (Fe_3Al) in order to compare the corrosion characteristics of Fe_3Al with that of stainless steels. It was observed that Fe_3Al exhibited passive behavior in electrolyte of pH 4, 8 and 12. Moreover, Fe_3Al exhibited cathodic loop in the polarization curve obtained in electrolyte of pH 12. Stable passivity was present in electrolyte of pH 4 and pH 8, and passivity was absent in electrolyte of pH 1.4, in which it showed active behavior. The passivity range was larger in electrolyte of pH 8 than that of pH 4. The polarization behavior of Fe_3Al in different electrolytes has been discussed considering Evans diagram based on the mixed potential theory. The passivation behavior, corrosion and pitting resistance of Fe_3Al was found superior compared to stainless steel in electrolyte of pH 8. However, the corrosion behavior of these materials was comparable in electrolyte of pH 4. Low oxygen aided the passive film formation in the case of iron aluminide whereas it did not for stainless steel, as larger passivity range and noble free corrosion potential were found for Fe_3Al in naturally aerated solution compared to aerated solution of pH 4. Chloride ions in electrolyte of different pH was observed to be detrimental to the pitting resistance of iron aluminide compared to stainless steel. The effect of Chloride ion on the passive film of Fe_3Al and stainless steels has been addressed.

The corrosion behavior of Fe_3Al alloyed with passivity enhancing elements M ($M = Cr$, Ti, Mo and Ta) was also investigated. It was found that the corrosion behavior of intermetallic $Fe_3Al - 5M$ was superior compared to that of

binary Fe_3Al in electrolyte of pH 4 and 8. The relative corrosion behavior of these Fe_3Al-5M intermetallics were found comparable. The $Fe_3Al-5Ta$ exhibited much better corrosion characteristics in electrolyte of pH 8 compared to others. Possible reasons for these observations are discussed.

TABLE OF CONTENTS

LIST OF FIGURES

LIST OF TABLES

CHAPTER 1

INTRODUCTION

Stainless steels have been popularly used as structural materials in corrosive environments. Apart from having sound mechanical properties, materials for structural applications must be resistant to corrosion. The corrosion resistance of stainless steels is due to the high degree of passive state stability conferred by the presence of chromium in them. The addition of Ni further stabilizes the FCC structure (austenitic stainless steel) and further imparts corrosion resistance. However, in some media like halide and sulfide solutions, this corrosion resistance is lost, as evidenced by the onset of intense localized attack, namely pitting. The susceptibility to pitting generally depends upon a combination of alloy composition and environment conditions. Replacement of stainless steels by iron aluminides has been considered in critical applications like coal based energy conversion systems, especially in sulfide environment or in aqueous solutions. This has been primarily due to the low corrosion rate and low cost of iron aluminide. Iron aluminides can also be used as the replacement of stainless steel in heat exchangers and in pilot plant molten systems for chemical air separation.

Iron aluminides based on Fe_3Al and FeAl compositions exhibit excellent oxidation and corrosion resistance because of their capability of forming protective alumina scales (Al_2O_3) in hostile environments, both at ambient and high temperatures. Ordered intermetallic alloys, although primarily used for their high temperature aqueous corrosion resistance, can also be advantageously utilized even at ambient temperature. Iron aluminides based on Fe_3Al have generated interest for many years due to

their potential oxidation and corrosion properties at relatively low cost. However, their poor ductility at room temperature has restricted their use, as they are difficult to fabricate into useful shapes.

The aim of the present work was to study the corrosion behavior of iron aluminide of composition Fe_3Al and compared it with that of stainless steels in aqueous solution of pH ranging between 1 and 12 in order to examine the effect of solution chemistry on the corrosion characteristics of these alloys. Another major aim of the study has been to evaluate the corrosion behavior of iron aluminide alloyed with passivity enhancing elements like Cr, Si, Ti, Mo, Ta, Nb, Ni and V in order to evaluate the effect of composition on the corrosion behavior of iron aluminide. The analysis has been carried out with the aid of potentiodynamic polarization technique. Their possible use as structural and construction material for corrosion resistance applications are also explored.

As regards organization of the thesis, Chapter 2 contains the literature review. The characteristics of iron aluminide and earlier work performed on the corrosion behavior of Fe_3Al have been discussed here. The experimental procedures have been presented in Chapter 3. The corrosion behavior of Fe_3Al, Fe_3Al-5M (M = Cr, Mo, Ti, Ta, Nb, V Ni and Si) and stainless steel have been presented and discussed in Chapter 4. The significant findings of the study have been summarized and the scope of future work outlined in Chapter 5.

CHAPTER 2

LITERATURE REVIEW

The search for new high temperature structural materials has stimulated much interest in ordered intermetallics. Aluminides of iron, nickel and titanium have been of particular interest. The attributes that make them attractive for high temperature applications are their low densities, relatively high melting points, and good high temperature strength. More important, they contain enough aluminium to form, in oxidizing environments, thin films of aluminium oxides that often are compact and protective [1].

2.1. IRON ALUMINIDES

The Fe_3Al based intermetallic alloys offer unique benefits of excellent oxidation and sulfidation resistance at a potentially lower cost than many stainless steels [2]. However, the application and development of these materials has been limited by their poor room temperature ductility and high temperature strength.

Studies of phase relationships in the Fe-Al system have confirmed the following equilibrium phases near the Fe_3Al composition [3,4]: a disordered solid solution (α), Fe_3Al with an imperfectly ordered B2 structure and an ordered DO_3 structure, and two phase regions of $\alpha+DO_3$ and $\alpha+B2$. The phase diagram [1] of Fe - Al system is shown in Figure 1. The DO_3 and B2 crystal structures are derivatives of the body centered cubic structure. These structures are presented in Figure 2 [1]. The transition temperature (T_c) between DO_3 and B2 in the binary Fe_3Al alloys is approximately 550^{o}C. In the present thesis, Fe_3Al would also be ordered as

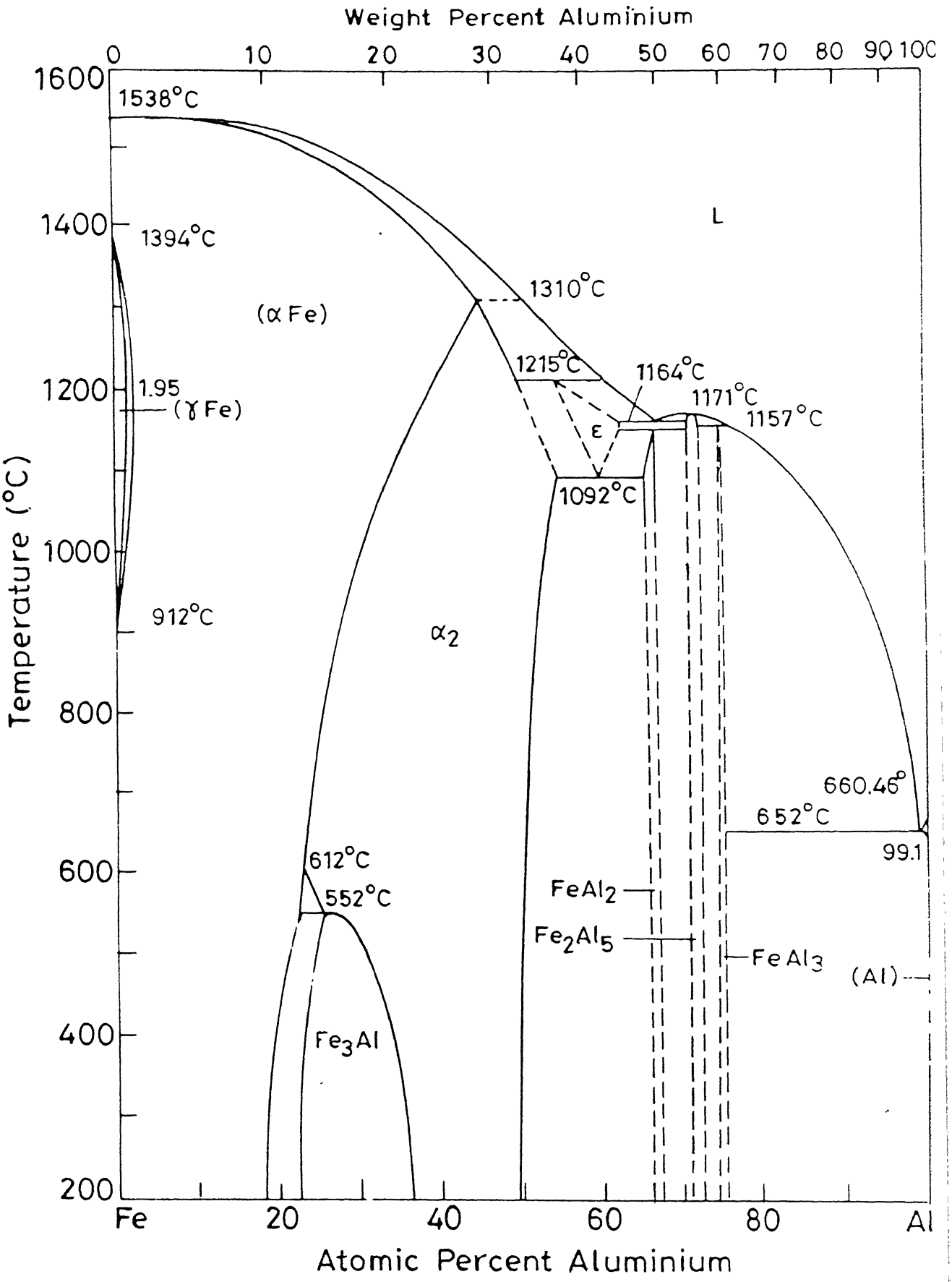

Figure 1 The Fe-Al phase diagram.

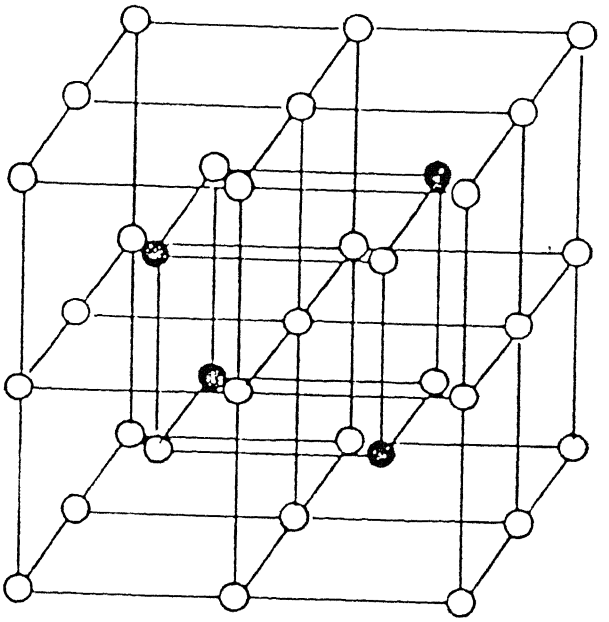

$Fe_3Al\ (DO_3)$

○ Fe ● Al

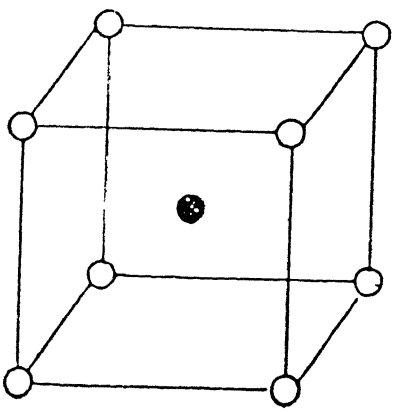

FeAl (B2)

Figure 2 The DO_3 and B2 ordered crystal structures of iron aluminides.

iron aluminide.

2.1.1 CORROSION OF IRON ALUMINIDE

Iron aluminide exhibits corrosion rates lower than stainless steels and other promising iron based alloys (including coating materials) by a couple of orders of magnitude as shown in Figure 3 when tested even in severe sulfidizing environment at 800°C [1]. It is noticed from the figure that the corrosion rate of stainless steel containing high amounts of Cr and Ni (Fe-25Cr-20Ni) is very high compared to Fe-Al alloys. Compositions based on Fe_xAl give lower corrosion rates as Al provides for a protective layer of alumina.

Janavicius and Payer [5] studied the corrosion behavior of iron aluminide Fe-Al in aqueous electrolytes of 1M NaOH, pH 10, 6, 4 and 1N Na_2SO_4. The corrosion of Fe-50Al was also compared to the behavior of Fe and Al using electrochemical and surface analytical techniques. Polarization curves, constant potential tests, scanning electron microscope (SEM), surface analysis using auger electron spectroscopy (AES) and X-ray photoelectron spectroscopy (XPS) were used to characterize the behavior. They found that aluminide exhibited behavior similar to Fe in all the solution In the NaOH solution, the aluminide was passive and corroded uniformly. In the Na_2SO_4 solution, the aluminide exhibited active-passive behavior but corroded in a localized manner (pitting). Pits grown in the pH 4 solutions had a lack of Fe in the center. The pit environment changed locally as Al corrosion products were present in small pits, but were absent near large pits. It was also found that passive films primarily contained Fe cations with few Al cations.

Buchanan and Kim [6] performed cyclic polarization experiments to

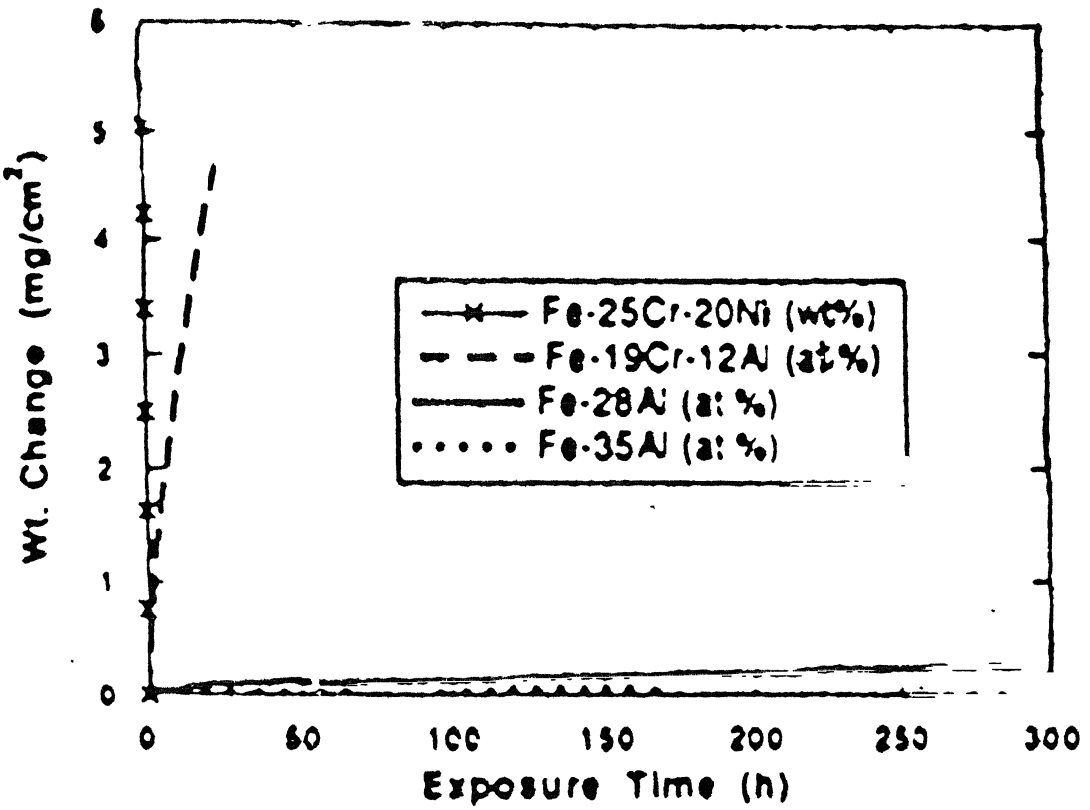

Figure 3 The weight gain vs time for FeAl alloys exposed to gas mixture with $p_{S_2} = 10^{-6}$ atm. and $p_{O_2} = 10^{-22}$ atm. at 800°C.

define the effects of chromium concentration (0-6 at%) and molybdenum addition (0-2 at%) on the aqueous corrosion behavior of iron aluminide containing 28 at% Al. They used an acid (H_2SO_4) chloride electrolyte of pH 4 containing 200 ppm chloride ion. From the corrosion study it was found, for the Fe-28Al composition, that cyclic anodic polarization testing indicated passivation, but with a relatively low breakdown potential for pitting corrosion, and a protection potential lower than the open circuit corrosion potential. Chromium additions alone proved beneficial by continuously increasing the pitting potential, as shown in Figure 4. It was observed that the breakdown potential increased with Cr content, indicating increased relative resistance to initiation of localized corrosion, which in their work was pitting corrosion. However, in all the cases (even in the intermetallic with the highest Cr content of 6 at%), the protection potential was still lower than the corrosion potential, indicating that pitting could initiate after an incubation period. Under free corrosion conditions Mo additions were found to raise the protection potential, such that at 1 and 2 at% Mo levels along with 4 at% Cr, the protection potential was higher than the free corrosion potential, indicating significantly improved resistance to initiation of localized corrosion. The overall results indicated that for satisfactory resistance to chloride induced localized corrosion, both higher Cr levels (4-6 at%) and Mo additions (1-2 at%) were desirable in Fe_3Al.

These two studies were the only available source in the literature and this was another reason for undertaking the work reported in this thesis.

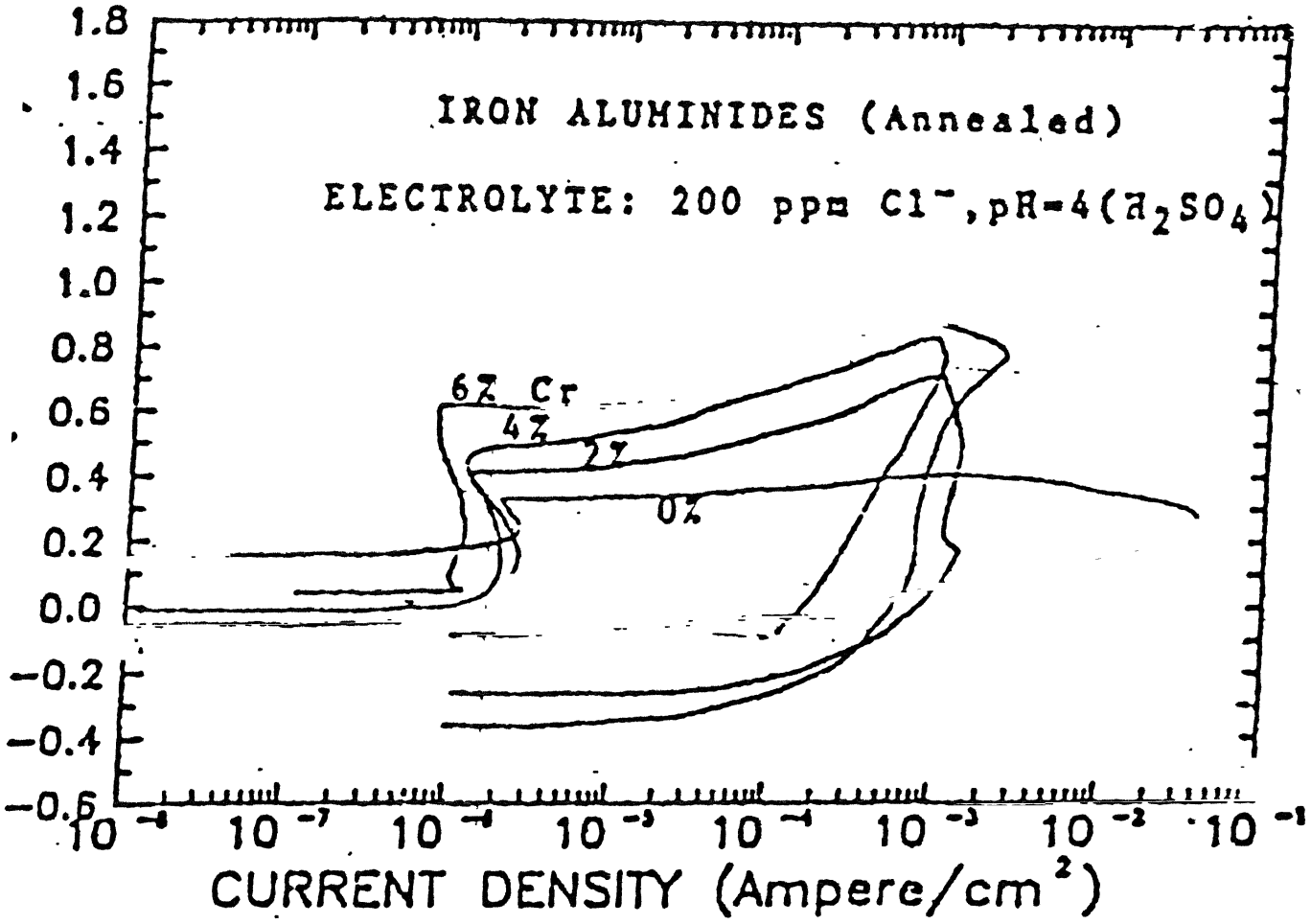

Figure 4 Cyclic anodic polarization behavior of ion aluminide in annealed aqueous H_2SO_4 solution containing 200 ppm Cl^- at pH = 4.

2.2.ELECTROCHEMICAL MEASUREMENTS

2.2.1.Potential Measurements

Potential measurements can be employed in a general manner to interpret corrosion phenomena as they can furnish information on whether the anodic or cathodic processes ,or both, are controlling corrosion. They can also provide useful information on film repair or film breakdown behavior on exposure to solution. In this method, basically the electrode potential of a corroding specimen is recorded as a function of time. However, these measurements cannot be used to predict or measure corrosion rate and this is the major limitation.

2.2.2.Polarization Measurements

During electrochemical corrosion, the anodic and cathodic process do not take place at their equilibrium potential. The deviation from equilibrium potential is called polarization. With the help of an external circuit, we can either accelerate the anodic or cathodic reaction by shifting the potential as explained below. A plot between the electrode potential and current density is known as anodic polarization curve in the former case and cathodic polarization curve in the latter.

The polarization behavior study can be performed by the following ways.

(i)Potentiostatic mode: In this mode, the working electrode's potential can be changed manually as desired by the operator in steps and the resulting current recorded.

(ii) Potentiodynamic mode: Probably the most sought after conventional mode in corrosion studies. The working electrode is subjected to an automatic potential scan at a preselected scan rate to allow one to obtain E-I relationship for a given metal/electrolyte system.

(iii)Galvanostatic mode: The current flowing between the specimen and a platinum auxiliary electrode is changed by using a variable resistance and the resulting potential measured.

(iv)Galvanodynamic mode: The current flowing between the specimen and a platinum auxiliary electrode is changed automatically at a preselected scan rate and the resulting potential stored.

For normal, metals both methods (potentiostatic/dynamic and galvanostatic/dynamic) give essentially the same result whereas for active-passive metals potentiostatic/dynamic curves are preferred as they yield more useful information about passivity.

Polarization curves are often used to measure the corrosion rate in either laboratory or plant. The determination of polarization curves is very quick and hence the corrosion rate of the specimen can be obtained swiftly. A complete curve can be usually determined in less than one hour in a laboratory setup, as compared to several days or weeks needed to measure corrosion rate by weight loss measurements. The corrosion of a metal expressed bycurrent density, can be converted to corrosion rate through Faraday's law using [7]

$$\text{Corrosion rate (mils/year)} = (1.24\text{x}10^{7} W_e / i_{corr})/D \quad (1)$$

$$(\text{mdd}) = (8.64\text{x}10^{7}) W_e / i_{corr} \quad (2)$$

where mdd = milligrams per square decimeter per day

1 mil = 0.001 inch

W_e = electrochemical equivalent (mg/coulumb)

D = density (gm/cm^3)

i_{corr} = corrosion current density (amp/cm^2)

2.3. CORROSION RATE DETERMINATION FROM POLARIZATION CURVE:

The polarization plots can be used to determine corrosion current density (i_{corr}). This can be obtained from the experimental polarization curves by mathematical analysis methods. Some of the methods used to finding the corrosion rate from the experimental curves are summarized below.

2.3.1. Four point method

Jankowski and Juchniewicz [8] have derived an expression for the determination of the corrosion current and tafel slopes from polarization data near the corrosion potential. The proposed method involves current estimation at four selected potentials and does not require knowledge of parameters other than the measured polarization curve. This four point method permits, in the majority of cases, the determination of the corrosion current more accurately and precisely than other methods.

In the four point method, the polarization curve is assumed to be describe by the equation

$$I = i_{corr} [\exp(E/\beta_{1a}) - \exp(-E/\beta_{2c})] \quad (3)$$

where E is the applied polarization i.e. $(E-E_{corr})$,

I is the applied current,

i_{corr} is the corrosion current,

β_{1a} is the Tafel slope of the partial anode reactions for the metal-ion/metal system and

β_{2c} is the Tafel slope of the partial cathode reactions for the second oxidation-reduction system on metal.

Algebraic rearrangement of the above Equation. gives

$$i_{corr} = \frac{I_1 I_{-1}}{(I_2 I_{-2} - 4 I_1 I_{-1})} \qquad (4)$$

$$b_{1a} = \frac{E}{\log\{\frac{I_1}{i_{corr}\,[1 - \exp(-E/B)}\}} \qquad (5)$$

$$b_{2c} = \frac{b_{1a}\, B \ln 10}{b_{1a} - B \ln 10} \qquad (6)$$

where I_{corr} = the corrosion current density

I_1 = the modulus of applied current at E,

I_{-1} = the modulus of applied current at -E,

I_2 = the modulus of applied current at 2E,

I_{-2} = the modulus of applied current at -2E,

β = parameter defined as $(1/\beta_{1a} + 1/\beta_{2c})^{-1}$

The corrosion current density (i_{corr}) and Tafel slopes (b_{1a}, b_{2c}) can be calculated after experimental determination of four current values at applied polarization equal to E, 2E (anodic polarization) and -E, -2E (cathodic polarization). One limitation of this method is that, for higher accuracy, the range of applied polarization E should be less than 50mV.

2.3.2. Coulostatic method

Kanno, Suruki and Sato [9] proposed a coulostatic method for determining Tafel slopes of corrosion reactions. In this method, a known amount of charge is supplied to the test piece and the overvoltage decay

curve recorded is analyzed to obtain the Tafel slopes. The anodic Tafel slope (β_a) can be obtained from

$$\beta_a = \frac{E}{\log_{10} \frac{t_3 - t_2}{t_2 - t_1}} \qquad (7)$$

where $E = E_1 - E_2 = E_2 - E_3 < 10$ mv and, E_1, E_2 and E_3 are the arbitrary values picked from the overvoltage decay curve and t_1, t_2 and t_3 are the corresponding times. Similarly, the tafel slope of the cathodic process (β_c) can be found out. I_{corr} can be then obtained with the aid of polarization resistance R_p using

$$I_{corr} = \frac{\beta_a \beta_c}{2.3 R_p (\beta_a + \beta_c)} \qquad (8)$$

In this method polarization resistance R_p can be found out by using equation

$$E_t = E_o \exp(-t/C_d R_p) \qquad (9)$$

where E_t = mean overvoltage at time t

E_o = overvoltage immediately after charging the double layer at time 0

C_d = differential double layer capacity of the test piece. Extrapolation of log E_t plot to t = 0 gives E_o value. Consider the relationship $C_d = q/E_o$, differential capacity C_d can easily calculated by using E_o values and the charge density q applied to test piece. Polarization resistance can be calculated from the slope of log E_t plot. The advantages of this method are the following.

The coulostatic method can be used without ohmic drop correction even in a high impedance solution. The time needed for the measurement is

considerably shorter compared to the usual electrochemical method.

2.3.3.Tafel extrapolation method

The experimental polarization curve of potential vs $\log i_{app}$ is curved at low overpotential but linear at high overpotential on a semi log plot. This is termed Tafel behavior. Experimental Tafel behavior defines the cathodic branch of half cell reduction reaction. The extrapolation of the region of Tafel behavior gives the corrosion rate, i_{corr} at E_{corr} as shown in Figure 5. Cathodic polarization data for iron in an acid solution, with extrapolation of the cathodic Tafel slope back to corrosion potential, E_{corr} is to obtain i_{corr} is illustrated in Figure 6. The intersection gives the corrosion rate or corrosion current density, i_{corr}. In order to determine i_{corr} by the Tafel extrapolation method, at least one decade of linearity on the semi log plots is desirable for maximum accuracy.

2.3.4.Linear Polarization Method

The measurable current that flows between the two electrodes is approximately linearly related to their potential difference, if the electrodes have a very small potential difference between them, within ±10 mV of the corrosion potential. Hence it is called Linear polarization. More importantly, the applied current density i_{app} is directly proportional to the corrosion rate through the equation[10]

$$\frac{dE}{i_{app}} = \frac{B}{i_{corr}} \qquad (10)$$

where dE is the potential difference between the two electrodes, B is a

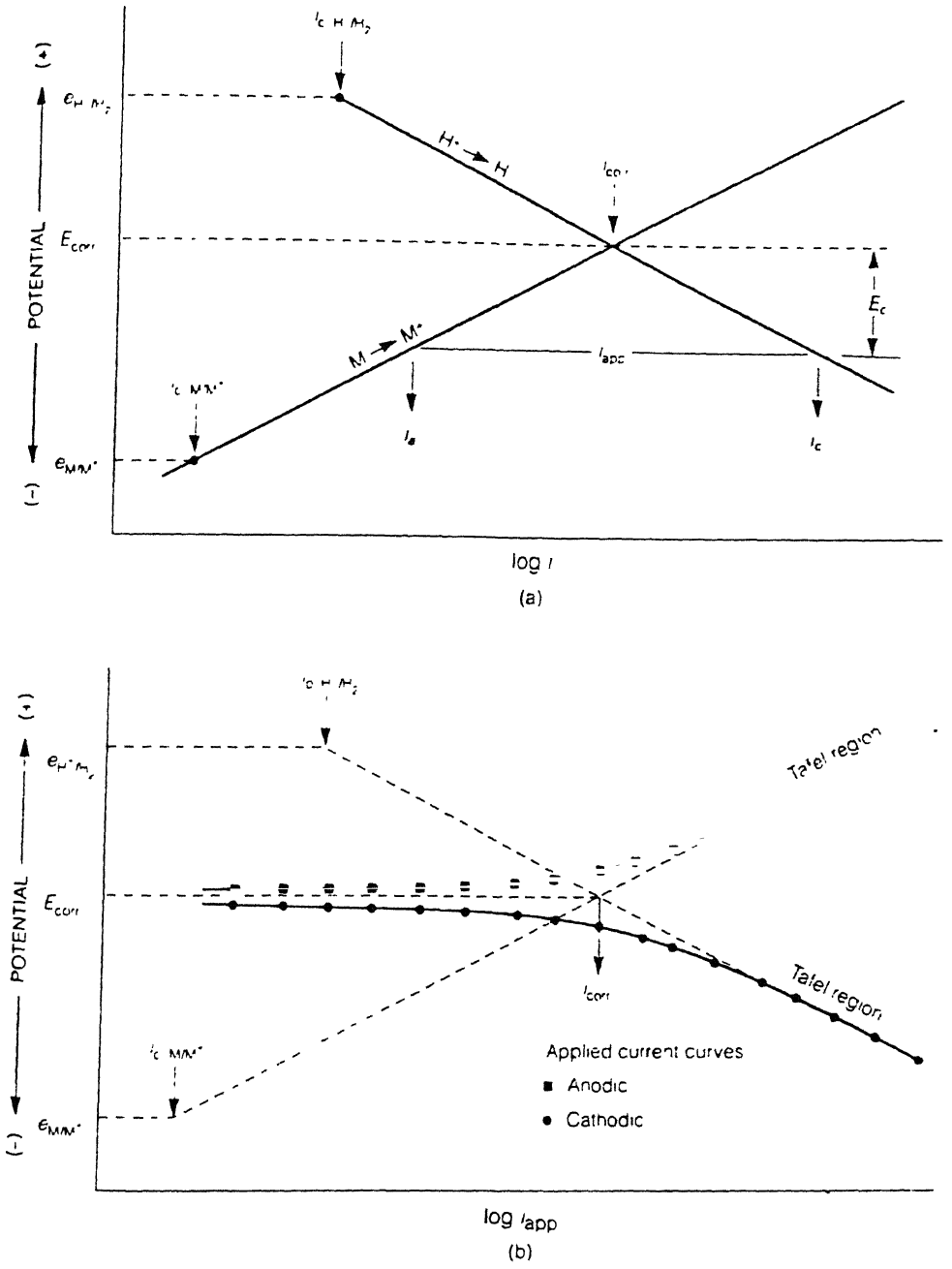

Figure 5 (a) Current density, i_{app}, applied to corroding electrode of E_{corr} and i_{corr} causing cathodic over voltage.

(b) Experimental polarization curve showing extrapolation of the region of Tafel behavior to obtain i_{corr}.

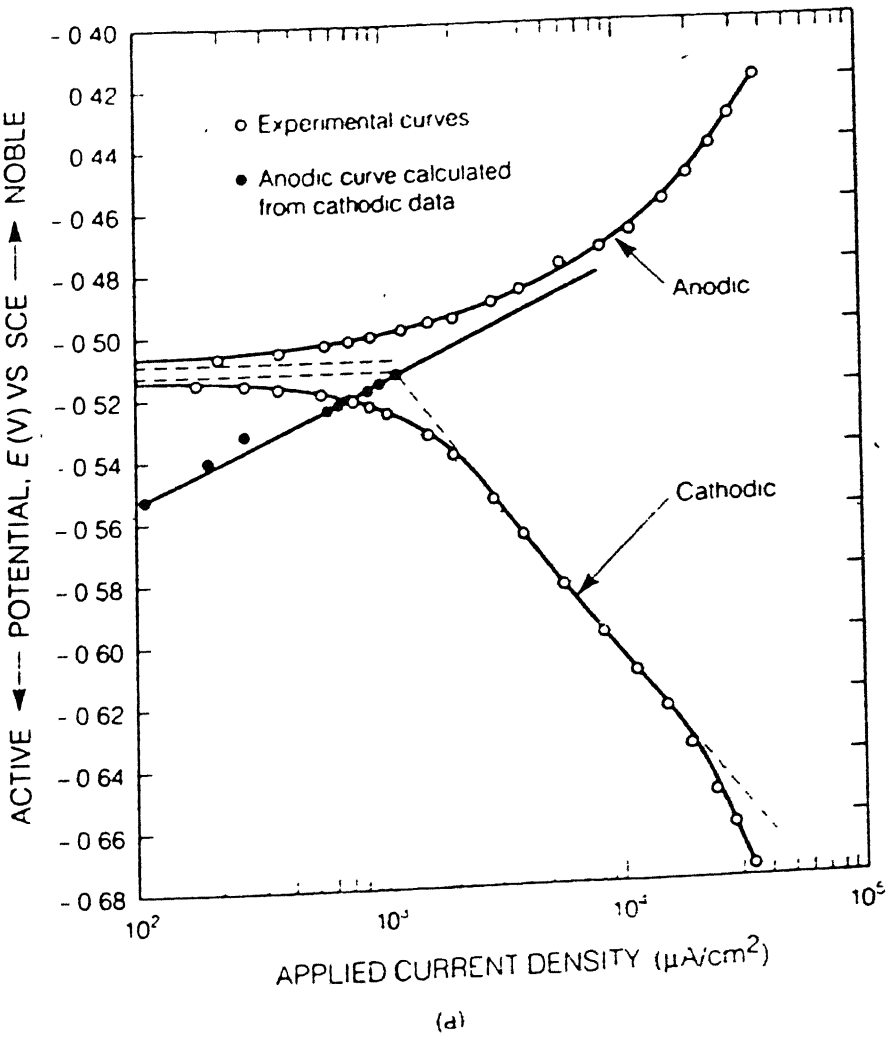

Figure 6 Polarization curves with extrapolation of cathodic Tafel slope back to E_{corr}.

constant, and i_{corr} is the current density that is directly proportional to corrosion rate by Faraday's Law, i.e.

$$\text{Corrosion rate} = i_{corr}/nF \qquad (11)$$

The constant B can be evaluated for each metal-environment corrosion system by calibrating the linear polarization measurements from result of weight-loss coupons, but more often B is just approximated, since it is about 0.02V for most corrosion systems.

This method is much more sensitive than weight-loss method if the corrosion rate is very low, and off course weight-loss might take months to develop any measurable weight loss while linear polarization method responds instantly.

Limitation: Since the linear polarization method measures the current flow through an electrolyte, anything that interferes with the current flow, such as an oil film on the probe , gives spurious results.

2.4. POLARIZATION BEHAVIOR ON PASSIVATING METALS

For metals exhibiting passivity, the potentiostatic or potentiodynamic methods give full information about passivation behavior. Figure 7 shows a typical potetiostatic/dynamic anodic polarization curve of a metal exhibiting passivity. The important points of this curve are described below.

A - corresponds to the equilibrium potential of the metal under given environment condition.

AB - anodic polarization behavior of a normal corroding metal.

B - corresponds to equilibrium potential for initiation of passive film growth E_{ip} .

C - at potential of primary passivation E_{pp} acceleration of metal

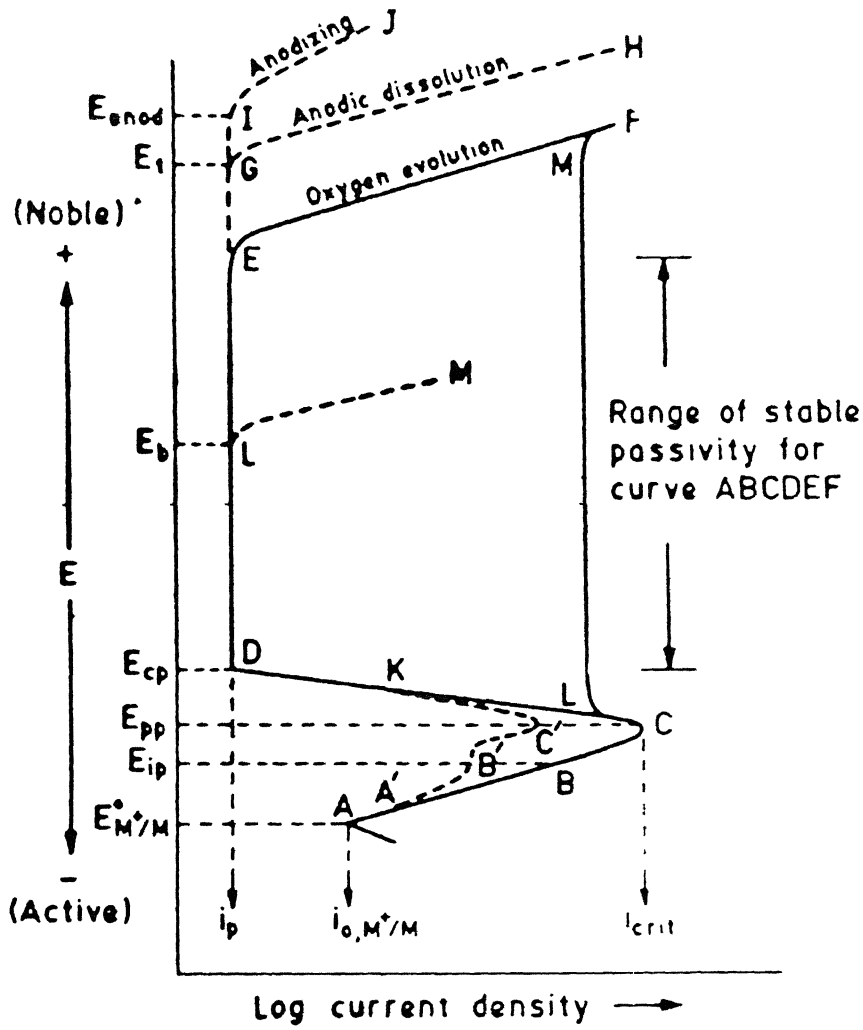

Figure 7 Anodic polarization curve of metal exhibiting passivity.

dissolution occurs.

At potential E_{pp} , the rate of protective film growth already exceeds the rate of its chemical dissolution and process of protective film formation begins.

D - at potential E_{cp} where formation of continuous protective film is completed and complete passivation is obtained.

DE - metal dissolution occurs at constant rate through the passivating oxide film.

E - end of passivity range and beginning of transpassivity

The relationship between the theoretical and measured experimental polarization curves can also be easily shown. Material will passivate spontaneously when the theoretical cathodic polarization curve intersects the theoretical anodic polarization at passive region only as shown in Figure 8 . This is the condition, when specimen passivates immediately on immersion in the electrolyte. This situation is most desirable for material construction.

Experimental polarization curve shows typical peak shaped curve,as shown in Figure 9. when theoretical cathodic curve intersects the anodic curve in the active region. Metal exhibiting this behavior corrode under given environment conditions. But they can be protected by application of anodic protection.

The experimental anodic polarization curve can also exhibits a cathodic current loop after the peak-shaped active to passive transition, as shown in Figure 10. This results when the cathodic curve intersects the theoretical anodic polarization curve in each of the active, partially passive, and passive region. Metals either exhibitshigh corrosion rates or

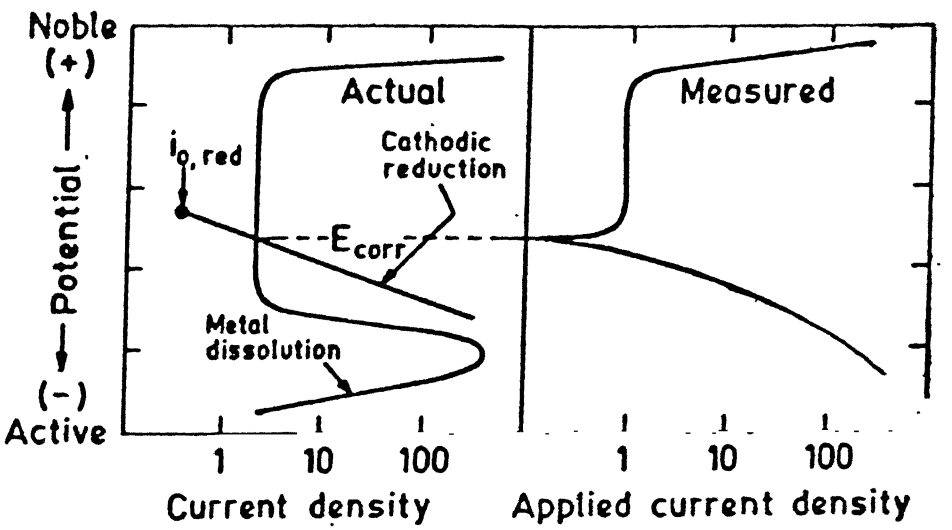

Figure 8 Actual and measured anodic polarization curves of a metal exhibiting passivity when passive state is stable.

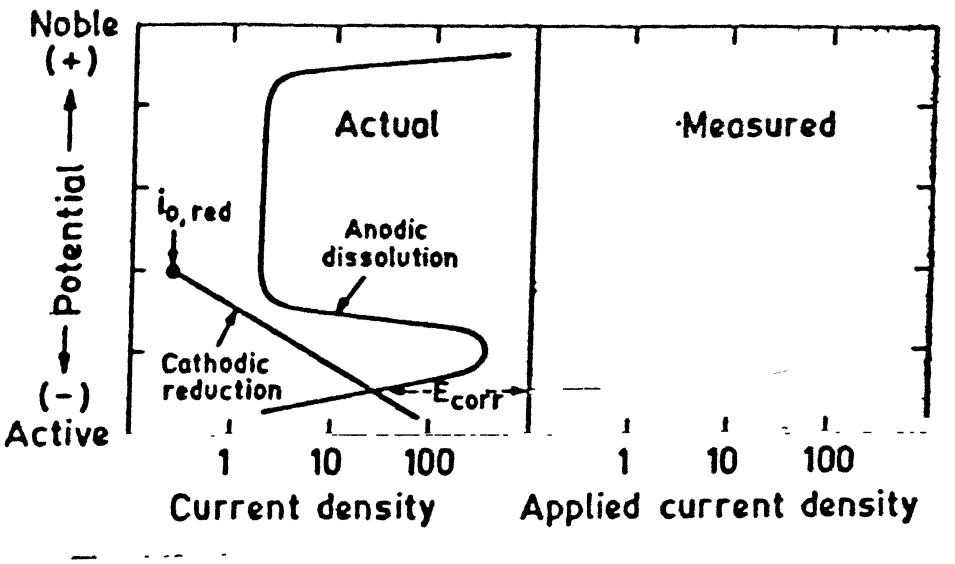

Figure 9 Actual and measured anodic polarization curves of a metal exhibiting passivity when active state is stable.

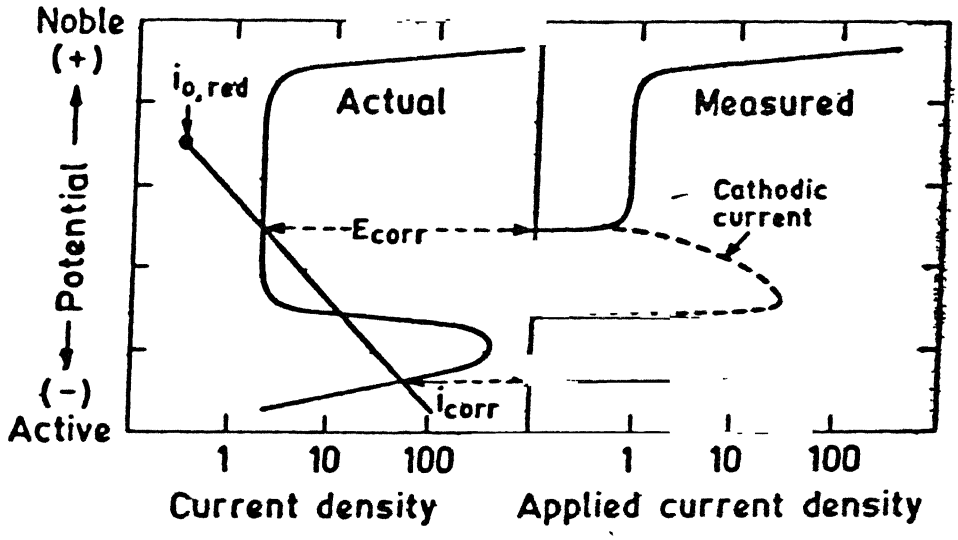

Figure 10 Actual and measured anodic polarization curves of a metal exhibiting passivity when both active and passive states are stable.

low corrosion rates, and are undesirable since a surface supposed to be passive can be rendered active by slight damage to the passive film. Once the surface becomes active it may not passivate again and corrosion can proceed to complete destruction of the material.

CHAPTER 3

EXPERIMENTAL PROCEDURE

This chapter describes the test specimen, its preparation, apparatus and electrolyte of various pH used, and the experimental methods employed in the study.

3.1. Test Specimen

A pancake of iron aluminide (Fe-28 at % Al) of diameter 120 mm and thickness 15 mm was obtained from the Defence Metallurgical Research Laboratory (DMRL), Hyderabad. This pancake was processesd by the ingot metallurgy route. In order to remove segregation, this pancake was homogenized at 1000^{o} C for 4 hours. A test piece of size 8cm x 4cm x 1.5cm was later ordered at 550^{o}C for 4 days. After ordering, specimens of size 1cm x 1cm and thickness of 3 mm were machined from this piece. Electric contact between sample and a (sealed) wire was taken care using cello tape and immediately mounted by cold mounting using a thermosetting resin which acted as an insulator for the other sides. Each mounted specimen was coarse ground initially with the help of an abrading belt and later polished with decreasing grit size of emery paper (1/0 through 4/0) and degreased with acetone before experiment. In case the same specimen had to be used for other studies, the surface was polished with emery paper to a 4/0 finish and degreased with acetone before each experiment.

It is considered good practice to increase the corrosion resistance of alloys by directly increasing their anodic polarization through alloying with elements of passive properties. Effect of alloying elements on the characteristic points of the potentiostatic curve of iron is shown in Table 1. Five atomic percent

Table 1 . Effect of alloying elements on the characteristic points of the potentiostatic curve of iron.

Alloying Element	i_p	i_{cp}	E_{pp}	E_{cp}	E_f	E_t
Cr	increase	decrease	increase	increase	decrease	S N D
Mo	decrease	increase	No Data	increase	decrease	S N D
Si	No Effect	decrease	No Effect	increase	decrease	decrease
V	decrease	increase	No Effect	No Effect	decrease	S N D
Ti	decrease	No Data	No Data	No Data	No Data	No Data
Nb	decrease	No Data	No Data	No Data	No Data	No Data

i_p = Passivation Current Density

i_{cp} = Complete Passivation Current Density

E_{pp} = Passivation Potential

E_{cp} = Complete Passivation Potential

E_f = Film Break Through Potential

E_t = Transpassive State Potential

S N D = Shift In Negative Direction

of passive inducing element Cr, Mo, Ti, Ta, Nb, V, Ni and Si of purity 99.9% was added to binary Fe_3Al to make new alloys of type Fe_3Al-5M (M = passivity inducing element). These alloys were melted in an electric arc furnace in an inert (argon) atmosphere. Each alloy was melted thrice to minimize segregation. These alloys were finally obtained in the form of buttons. These buttons were homogenized at 1000°C for 4 hours, before processing, to further minimize segregation. All buttons of Fe_3Al-5M were processed before preparing corrosion specimen according to the following flow sheet:

Starting Buttons (Fe_3Al-5M)

|

Homogenized at 1000°C for 4 hours

|

Rolled at 1000°C

|

(Deformed Thin Strips)

|

Machined to size 1cm x 1cm

|

corrosion specimen

The stainless steels (304, 310 and 316) were obtained in the form of rod of dia 20mm. The compositions of these stainless steels are given in Table 2 Specimens of dia 11.2 mm and thickness 3 mm were machined from these rods, so that the mounted sectional area would be of 1 cm^2 with an accuracy of ±1%, as specified by ASTM [11]. The corrosion specimen were mounted as described before.

Table 2 Composition of stainless steels used in present study

Specimen	Carbon (C)	Manganese (Mn)	Silicon (Si)	Nickel (Ni)	Chromium (Cr)	Molybdenum (Mo)
SS 304	0.08	2.00	0.75	8.00	18.00	—
SS 310	0.25	2.00	0.75	19.00	24.00	—
SS 316	0.08	2.00	0.75	10.00	16.00	2.00

3.2 Apparatus

The main apparatus used for the polarization experiments were a polarization cell equipped with a facility of bubbling nitrogen/air and a potentiostat (Vibrant Potentiostat/Galvanostat VSM/PG/30) interfaced to a computer (NEC PC 80386) attached with a printer (EPSON FX-80). The potentiostat used in the study was capable of performing a wide variety of potentio and galvano functions required for basic and applied studies in the field of corrosion. Repeatable results were obtained as long as studies did not require a compliance voltage greater than ±30V (d.c.). The cell potential would be controlled within ±4V. However, one limitation of the potentiostat was that it would not measure currents below 1 microamperes and therefore the instrument sensitivity limit is indicated in all the experimental polarization diagrams to be presented later. In order to acquire polarization curves by the computer system, current and potential measurements had to be converted to digital form by a two channel analog-digit converter. Two digit digital display meters (one for potential and the other for current) were fixed on the front panel to visually aid to note down readings manually during simply steady state experiments or with slow ramping rates. The experimental arrangement is schematically illustrated in fig 11

The polarization cell used in the study is shown in Fig 12. A round-bottom flask had been modified by the addition of various necks to permit the introduction of electrodes, gas inlet and outlet tubes, and a thermometer. The Luggin probe connected with KCl salt bridge separated the bulk solution from the saturated calomel reference electrode (SCE). The probe tip could be easily adjusted to bring in close proximity with the

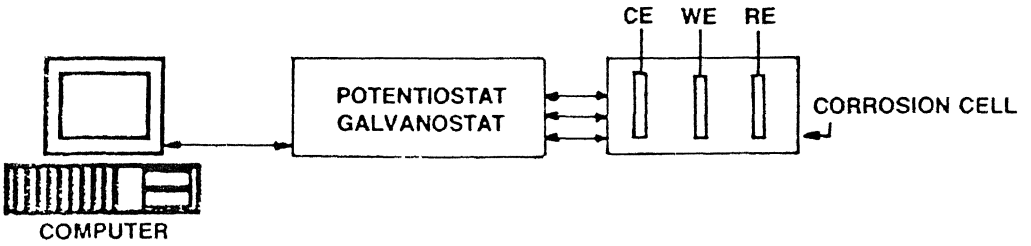

Figure 11 Computer assisted instrumentation employed in the present study.

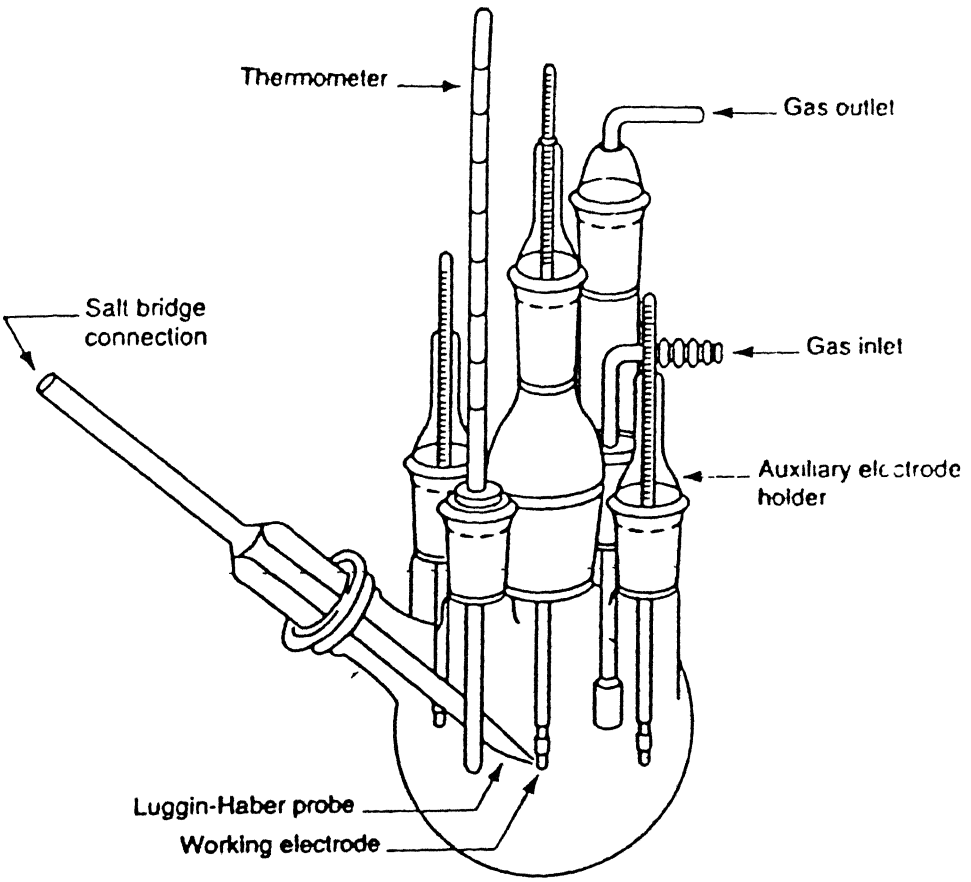

Figure 12 Electrochemical polarization cell used for conduction polarization studies.

working electrode. The three electrodes used are the working electrode (mounted specimen connected with a wire), the counter electrode (high-purity platinum flat stock wire), and the reference electrode (saturated calomel electrode with E^{o}= +0.242V vs standard hydrogen electrode), as per the ASTM recommendations [11]. The potential of the calomel electrode was checked at periodic intervals to ensure the accuracy of the potential of the electrode.

3.3 Electrolyte

The following electrolytes were used in the present study to evaluate corrosion behavior of stainless steel 304, 310, 316, Fe_3Al and Fe_3Al-5M intermetallic.

(a) 0.1N H_2SO_4 (pH 1.4) with and without 200 ppm of Cl^-

(b) Aqueous solution of H_2SO_4 of pH 4 with and without 200 ppm of Cl^-

(c) Aqueous solution of NaOH of pH 8 with and without 200 ppm of Cl^-

(d) 0.1N NaOH (pH 12) with and without 200 ppm of Cl^-

Electrolyte of different pH (1.4, 4, 8, and 12) were made with distilled water and reagent grade chemicals. The solution 0.1N NaOH and 0.1N H_2SO_4 had pH of 12 and 1.4 respectively. Electrolyte for pH 4 and pH 8 were adjusted by adding distilled water in 0.5N H_2SO_4 and 0.01N NaOH solution, respectively. Electrolyte containing 200 ppm of Cl^- was made by addition of 0.65 gms of NaCl in 1000 ml of solution.

A fixed volume of 1000 ml of test solution was used for all the tests. Although ASTM recommends 40 ml of test solution to every 1 cm^2 area of test surface [11], it is also recommended to keep the ratio of the solution volume to specimen surface area high in order to avoid any appreciable change in the corrosivity of the solution during the test,

especially since the solution would not be recirculated [11]. Only test solutions that was less than a week old wereused in order to minimize contamination of the electrolyte. Additional care was taken to stir the solution thoroughly before starting each test.

3.4 Test Procedure

The electrolyte solution (1000 ml) was transferred to corrosion cell. The electrodes were immersed in the electrolyte and secured in place using a retort stand. Precaution was taken to ensure that the specimen was immersed to a depth of not less than 2 cm from the liquid/air interface and the luggin probe was adjusted so that its tip was consistently two times the tip diameter (10 mm) away from the working electrode. All these precautions were necessary to ensure that the oxygen supply was identical and adequate for all the specimens. Different aeration treatments were studied. Aeration was maintained by bubbling oxygen (purity 99%) and deaeration by bubbling argon (purity 99%) through the solution during the course of experiment and for 2 hours before the start of each new experiment. It was seen that aeration shifted the corrosion potential to active side as compared to normal and also decreased the passivity range of iron aluminides. Therefore, for consistency, the test solutions used for all the experiments in this study were naturally aerated.

In polarization measurements, the portion of the electrolyte between the working electrode and the capillary tip of the reference electrode also contributes towards the electrical resistance. Since resistance is a function of the distance between the electrodes, better accountability for the measured values was achieved by keeping the gap as small as possible to minimize the extra resistance.

The corrosion potential of the working electrode was continuously recorded staring immediately after immersion until a constant potential was obtained. Potentiodynamic polarization studies were conducted immediately after stabilized corrosion potentials values were obtained. The period for stabilization depended upon the specimen, its surface finish, and electrolyte. Generally, it took 4-5 hours for obtaining a constant potential. Although the effect of scan rate was initially studied, all the other tests were conducted with a potential scan rate of 1 mV/sec. Data were collected at every 30 sec interval until breakdown occurred or until the potential of 2V was reached, whichever was earlier. Generally the total duration of the test was 6 hours.

Experiments in noise mode (measurement of free corrosion potential) were first conducted for all the specimen (intermetallic Fe_3Al, Fe_3Al-5M and stainless steel) in electrolyte of different pH. Potentiodynamic polarization experiments were conducted after stabilizing the free corrosion potential in noise mode in each case.

CHAPTER 4

RESULTS AND DISCUSSION

In this chapter the corrosion behavior of iron aluminides (binary Fe_3Al and alloyed Fe_3Al-5M) and stainless steels are presented and discussed. The effect of scan rate, solution aeration/deaeration, pH and composition on the corrosion characteristics (free corrosion potential and polarization behavior) of these materials are discussed.

4.1 EFFECT OF SCAN RATE

The potentiodynamic polarization curves of binary iron aluminide (Fe_3Al) in 0.1N H_2SO_4 solution of pH 1.4 as a function of scan rate are presented in Figure 13. The zero current potential ZCP (i.e., the potential at which current density approaches zero or reverses sign on scanning) decreases with increasing scan rate as more negative zero current potentials were obtained at higher scan rates. The ZCP and the potentiodynamic behavior did not change for scan rates below 1mV/s. This behavior can be explained as follows. At higher scan rates, the time for formation of surface films in the electrolyte was shorter. It is quite possible that the formation of oxide film did not either cover the entire surface area or the oxide that formed was lower than the equilibrium thickness at higher scan rates. Therefore, ZCP was established at active potentials at faster scan rates. As the scan rate was decreased, the time for the formation of oxide (surface) film increased and below a certain scan rate, sufficient time was available for providing an oxide film for complete equilibrium coverage of the entire surface. Therefore, the ZCP remained constant below a certain scan rate as expected and this has been

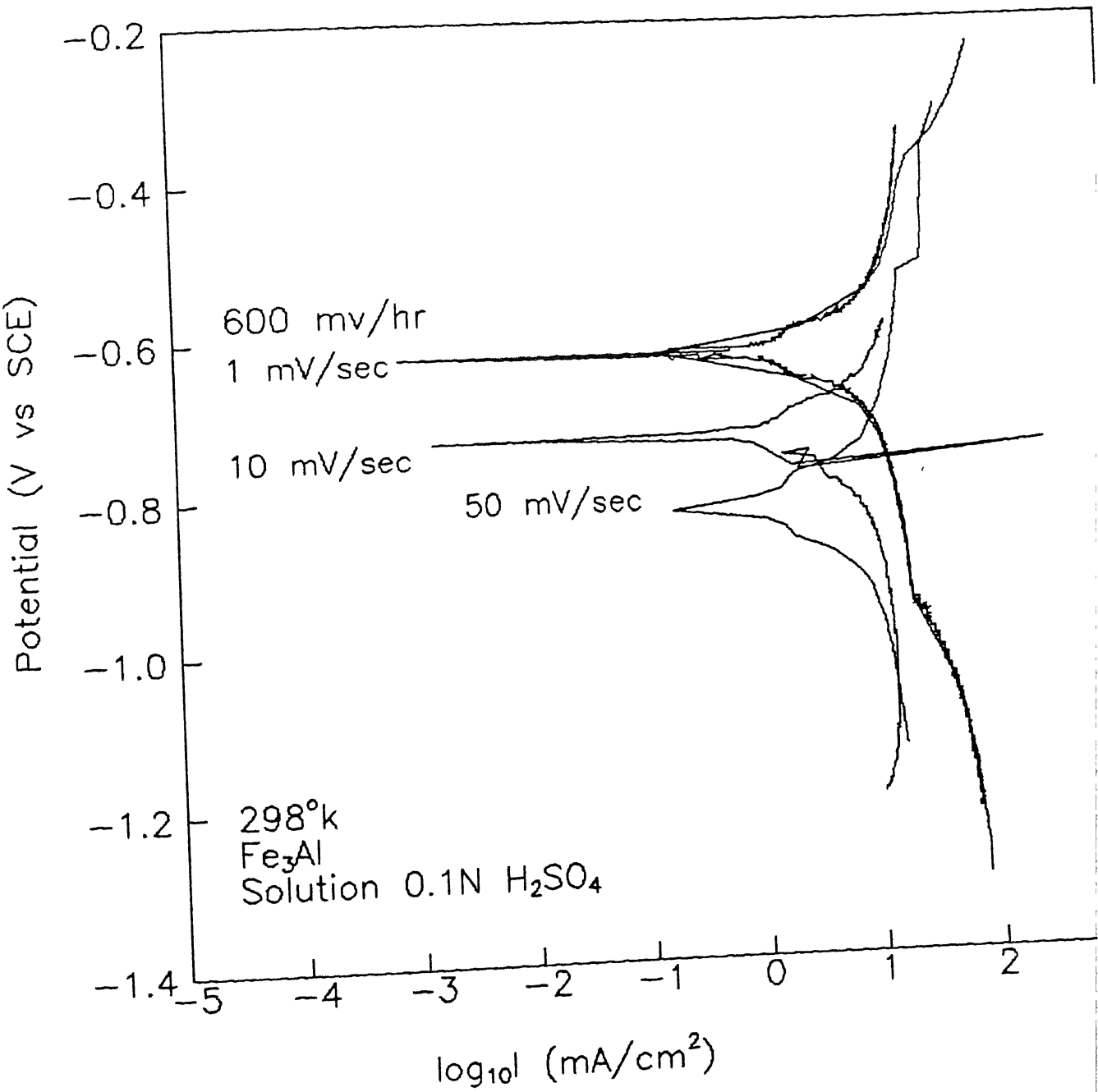

Figure 13 Effect of scan rate on polarization behavior of iron aluminide (Fe_3Al) in 0.1N H_2SO_4 solution.

observed in the present study. A constant scan rate of 1 mv/s was selected for all the studies conducted further.

4.2 EFFECT OF SOLUTION AERATION/DEAERATION

4.2.1 Electrolyte of pH 1.4

The free corrosion potential, FCP (i.e., electrode potential on immersion in electrolytes) of iron aluminide as a function of time in 0.1N H_2SO_4 of pH 1.4 for iron aluminide (Fe_3Al) under different solution aeration conditions are presented in Figure 14. The FCP started from a more negative value (active side) and stabilized at a noble value for all the cases of solution aeration conditions. The stabilized FCP was not the same for different aeration conditions. The FCP was slightly noble in the deaerated solution as compared to other solution conditions. This behavior can be explained as follows. The material on immersion initially reacts with the electrolyte. The FCP tending to noble values with time indicates that there was formation of a protective oxide film at the surface. The FCP was finally stabilized when the equilibrium corrosion behavior was established through the surface film. It is known that in case of aluminium, the passive film is stable even at potential characteristics of deaerated conditions [12]. This could be the reason for the FCP of iron aluminide exhibiting noble values in deaerated condition compared to normal and aerated condition.

The potentiodynamic polarization curves for iron aluminide in 0.1N H_2SO_4 of pH 1.4 as function of solution aeration (normal, aerated and deaerated conditions) are shown in Figure 15. The ZCP exhibited a noble value in deaerated condition compared to other conditions. Moreover, the ZCP for normal solution condition was noble compared to that for the

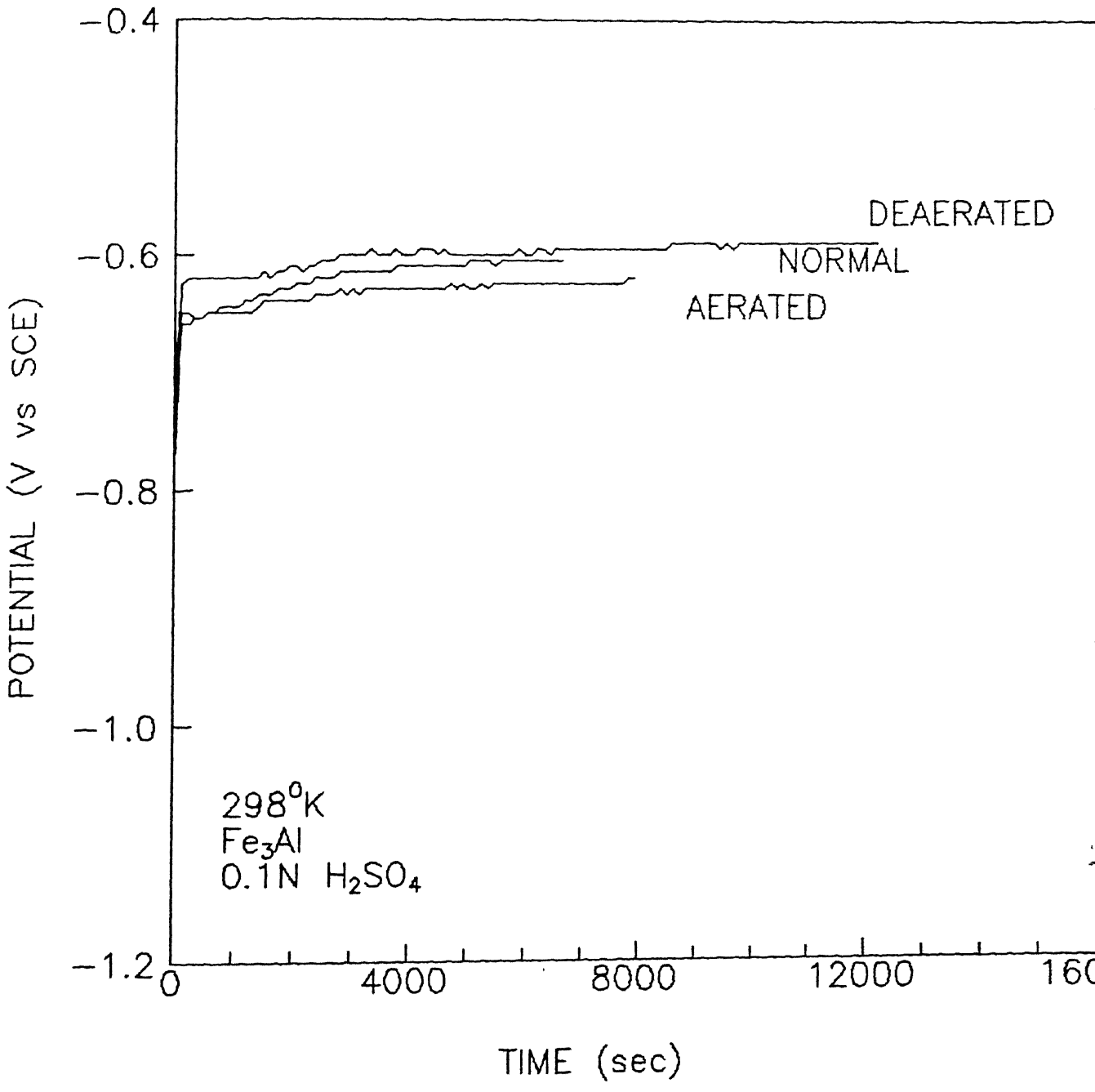

Figure 14 Effect of solution aeration/deaeration on the free corrosion potential as a function of time for Fe_3Al intermetallic in 0.1N H_2SO_4.

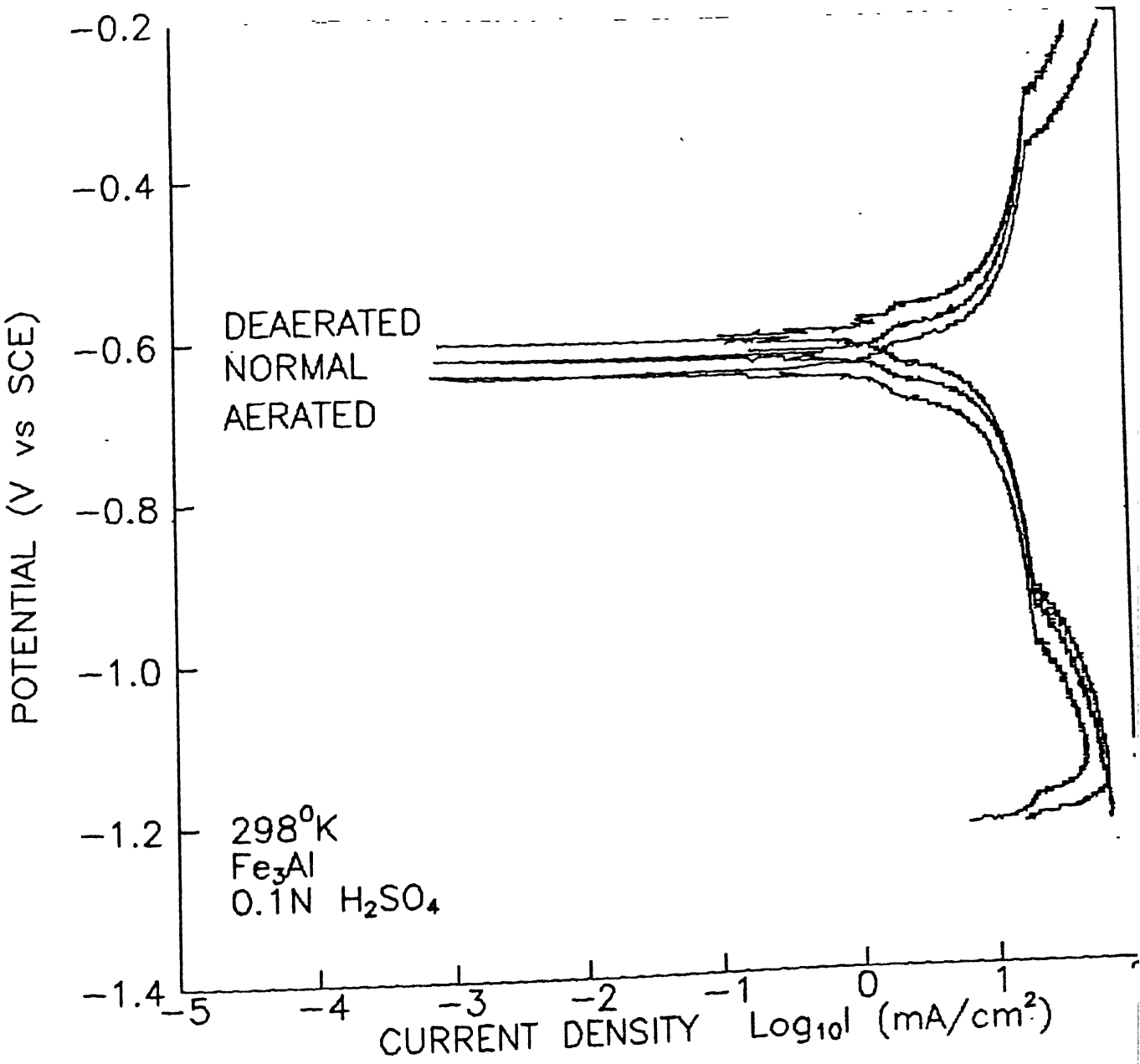

Figure 15 Effect of aeration/deaeration on the potentiodynamic polarization behavior of Fe_3Al in 0.1N H_2SO_4.

aerated solution. This behavior was similar to the respective stabilized FCP in differently aerated solutions (Figure 14). The corrosion characteristics of iron aluminide in different conditions (aerated, deaerated and normal) are summarized in Table 3. The corrosion rate i_{corr} was obtained by the linear polarization method. The corrosion rate was found to be the minimum in the deaerated solution. Aeration increased the corrosion rate, with naturally aerated solution showing the maximum corrosion rate. The formation of protective surface film was different in different aerated condition. The reason for enhanced corrosion in aerated solution could possibly be explained by considering additional cathodic reduction reactions becoming operational with the addition of more oxygen in the solution, for example, oxygen reduction reaction. It is also quite possible that in aerated solution excess oxygen would have caused the formation of soluble oxide(s), which could have enhanced the corrosion rate. Therefore, in aerated and normal solution corrosion rate was high compared to deaerated solution.

4.2.2 Electrolyte of pH 4

The FCP of iron aluminide as function of time in H_2SO_4 electrolyte of pH 4 in normal and aerated conditions is presented in Figure 16. In this electrolyte, the FCP started from an active value and

Table 3 Corrosion characteristics Fe_3Al in different solution condition

(Aerated deaerated and normal)

solution condition	Free corrosion potential (mV vs SCE)	Zero current potential (mV vs SCE)	Current density ($\mu A/cm^2$)	Corrosion rate (MPY)
Deareated	-591	-595	156.99	70.67
Normal	-607	-615	208.91	94.05
Aerated	-625	-659	187.83	84.55

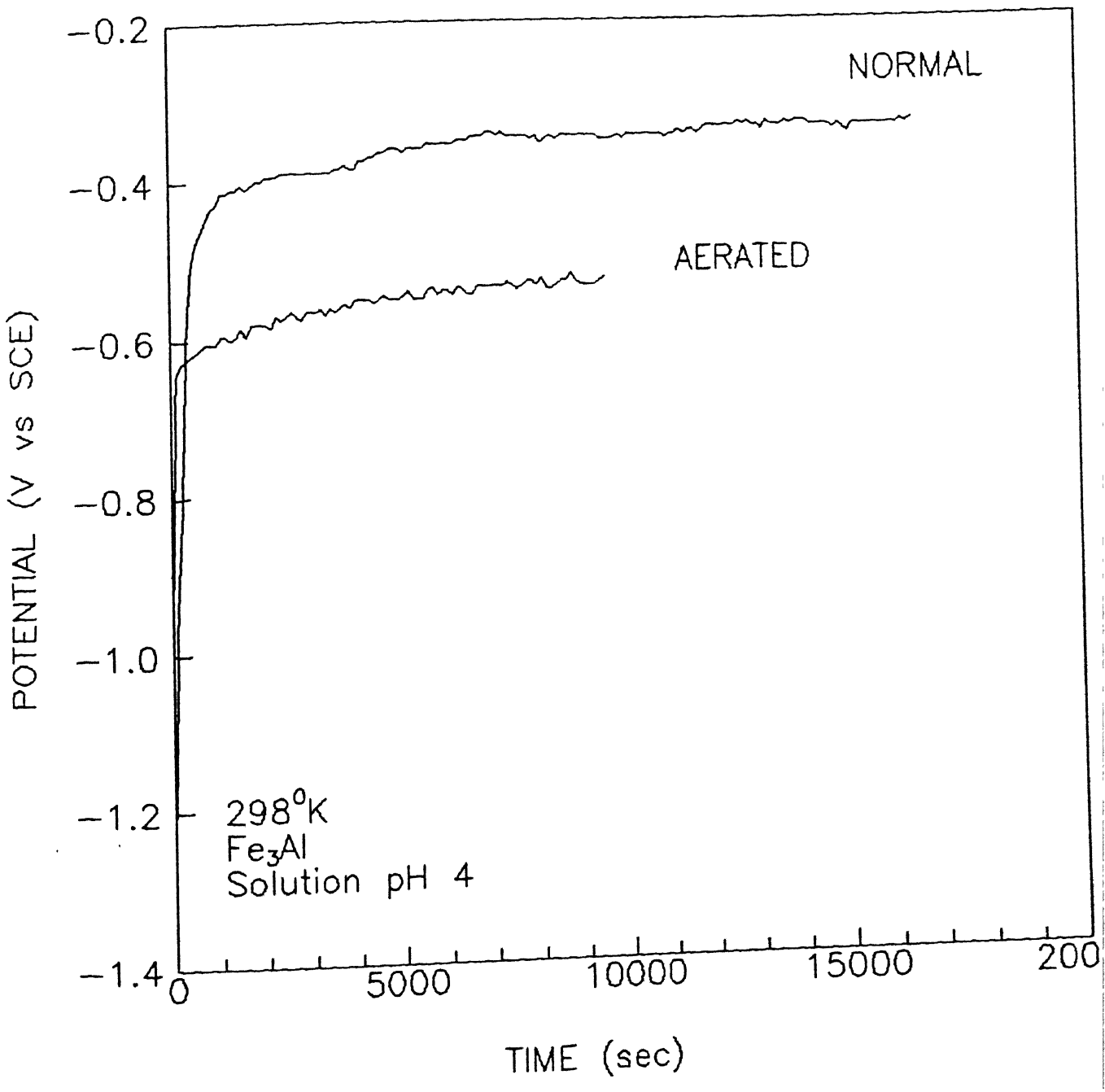

Figure 16 Effect of solution aeration on the free corrosion potential of Fe_3Al as a function of time in H_2SO_4 electrolyte of pH 4.

stabilized at a noble value for both the cases. Moreover, the stabilized FCP in the normal solution was noble compared to that in the aerated solution, as observed in 0.1N H_2SO_4 (pH 1.4) solution, earlier.

The potentiodynamic polarization curves for iron aluminide in normal and aerated H_2SO_4 electrolyte of pH 4 are presented in figure 17. It can be observed from the figure that iron aluminide exhibited passive behavior in the naturally aerated electrolytes and the passivity range was larger compared to that in the aerated electrolyte. Active behavior was observed in the case of aerated electrolyte.

In order to undertand the observed behavior, the effect of oxidizer concentration on the corrosion behavior of an active-passive alloy is first considered. The effect of increasing oxidizer concentration on corrosion of an active-passive alloy can be explained by the Nernst equation.

$$E = E^0 + \frac{RT}{nF} \ln \frac{\text{product of activities of reactants}}{\text{product of activities of products}} \qquad (12)$$

The cathodic reduction reaction may be evolution of hydrogen from acid or neutral solution according to the following equations.

$$2H^+ + 2e^- \longrightarrow H_2 \text{ (acid solution)} \qquad (13)$$

$$2H_2O + 2e^- \longrightarrow H_2 + 2OH^- \text{ (neutral and alkaline solution)} \qquad (14)$$

or reduction of dissolved oxygen in acid or neutral solutions according to

$$O_2 + 4H^+ + 4e^- \longrightarrow 2H_2O \text{ (acid solutions)} \qquad (15)$$

$$O_2 + 2H_2O + 4e^- \longrightarrow 4OH^- \text{ (neutral and alkaline solutions)} \qquad (16)$$

Taking the general equation for a half cell reaction as

$$aA + mH^+ + ne^- \longrightarrow bB + dH_2O \qquad (17)$$

and applying the Nernst equation, we obtain

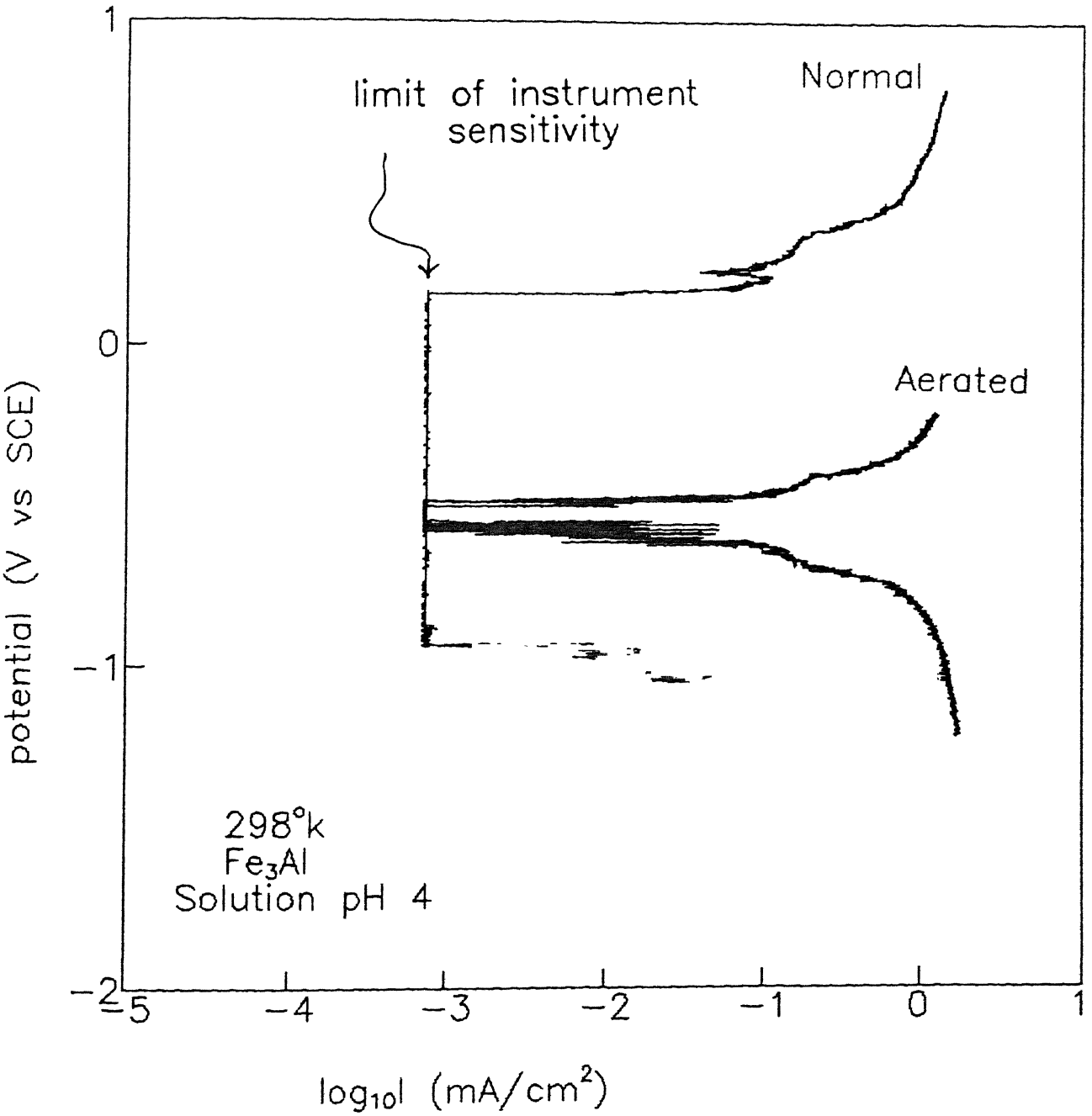

Figure 17 Effect of aeration on the potentiodynamic polarization behavior of Fe_3Al in H_2SO_4 electrolyte of pH 4.

$$E = E^{o} + \frac{RT}{nF} \ln \frac{(A)^{a}(H^{+})^{m}}{(B)^{b}(H_2O)^{d}}$$

It can be seen from the above equation that electrode potential becomes more positive (noble) as activities of oxidized species (A) and (H^{+}) increases. Therefore, an increase in the oxidizer concentration (O_2) lead to upward shifting of reduction potentials and consequently the cathodic polarization curve. As can be seen from Figure 18 oxygen concentration corresponding to cases 1, 2, 7 and 8 should result in experimental polarization curves exhibiting active behavior while that corresponding to 4, 5 and 6 should exhibit active/passive behavior. With the aid of the above theory, the possible reason for the difference in potentiodynamic polarization curves in the aerated and normal solutions in H_2SO_4 electrolyte of pH 4 can be understood. As the FCP in the normal solution was noble compared to the aerated solution (Figure 16), it is reasonable to assume that the schematic anodic polarization curve in the naturally aerated solution would be shifted in the noble direction compared to the anodic polarization curve of the aerated solution. This is shown schematically in Figure 19. The experimental polarization curve was obtained by the addition of cathodic and anodic polarization curves. Thus, on applying the mixed potential theory, by the addition of cathodic and anodic curves, the experimental corrosion behavior of iron aluminide in normal and aerated solution, (Figure 17) can be explained as shown in schematically in Figure 19.

4.3 CORROSION OF IRON ALUMINIDE AS A FUNCTION OF pH

The FCP of iron aluminide as function of time in electrolytes of

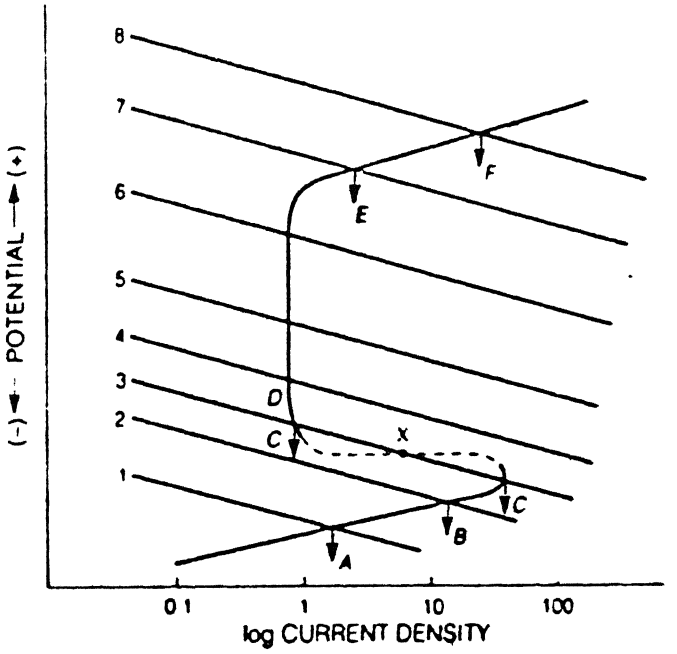

Figure 18 Effect of oxidizer concentration on corrosion behavior of an active-passive alloy.

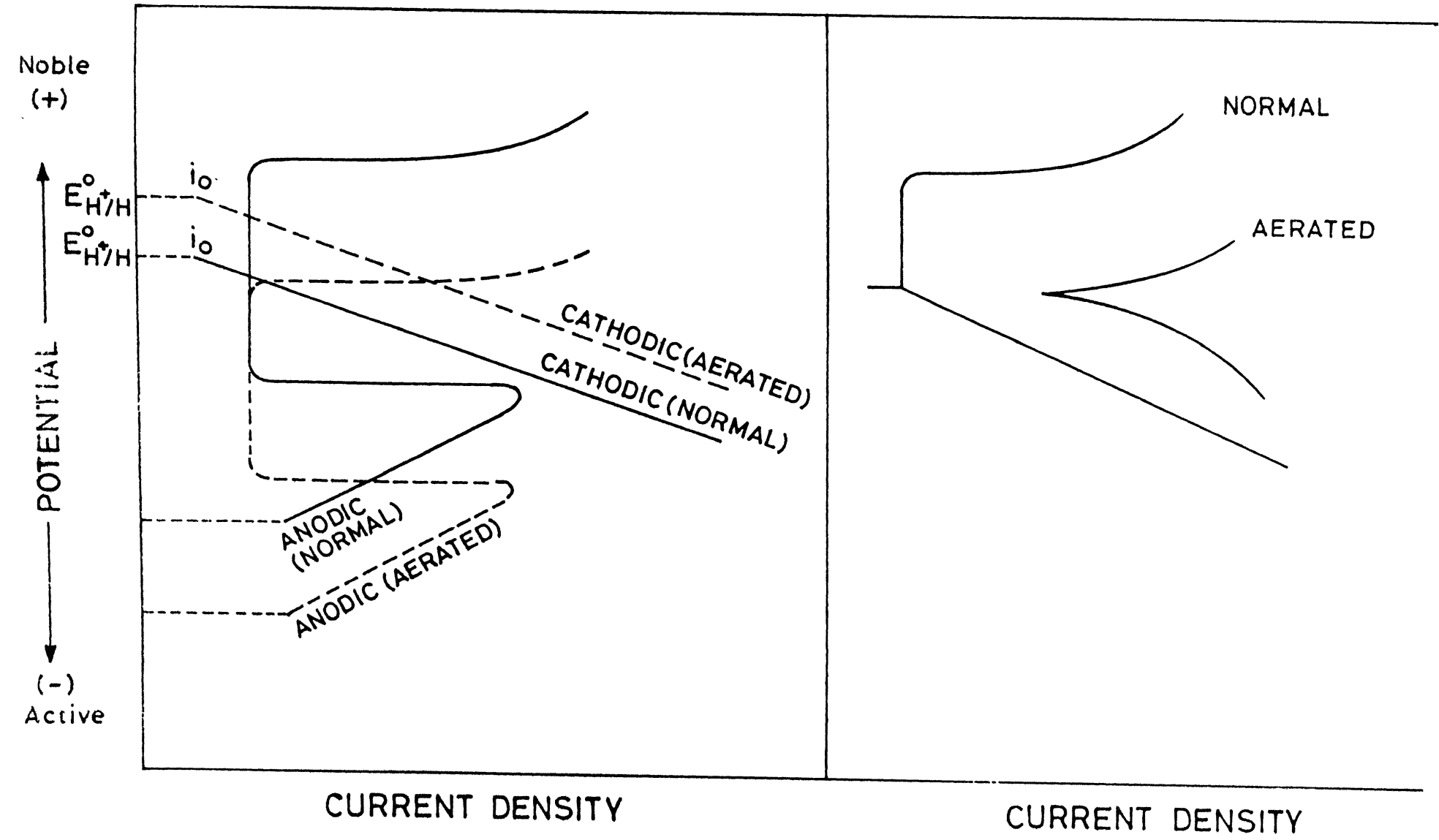

Figure 19 Schematic Evans diagram based on mixed potential theory explaining corrosion behavior of Fe_3Al in normal and aerated H_2SO_4 solution of pH 4.

pH 1.4, 4, 8 and 12 are shown in Figure 20. In all the electrolytes, the FCP started from an active value and stabilized at a noble value. Moreover, stabilized FCP in NaOH electrolyte of pH 8 was noble compared to that in other electrolytes.

The potentiodynamic polarization curves of iron aluminide in electrolytes of different pH are presented in Figure 21 and the corrosion characteristics are summarized in Table 4. It can be observed from Figure 21 that iron aluminide exhibited passive behavior in all the electrolytes except in electrolyte of pH 1.4 in which case it exhibited active behavior. Moreover, the polarization curve for pH 12 exhibited active/passive behavior with cathodic loop. Stable passivity was present in electrolyte of pH 4 and 8, whereas it was absent in electrolyte of pH 1.4. The passivity range was larger in electrolyte of pH 8 than that of pH 4. The above experimental results can be explained as follows.

The product of aqueous corrosion would be either soluble or insoluble compounds. Soluble compounds usually enhance corrosion by increasing the conductivity of the electrolyte and by allowing corrosion to take place by not providing a barrier. Insoluble compounds may precipitate either on the anode or cathode or somewhere in between, depending on the relative mobilities of the ions produced at the anode and cathode [10]. A layer of corrosion products on the corroding metal, even if it is porous and imperfect like rust scale, will slow down corrosion by slowing the diffusion of the react ants and by slowing the diffusion of the metals ions from the anode. If it completely covers the surface then it acts as a passive layer. Therefore, it can be first concluded that there is a passive film forming on iron aluminides in electrolytes of pH 4, 8 and 12.

The experimental polarization curves in different electrolytes

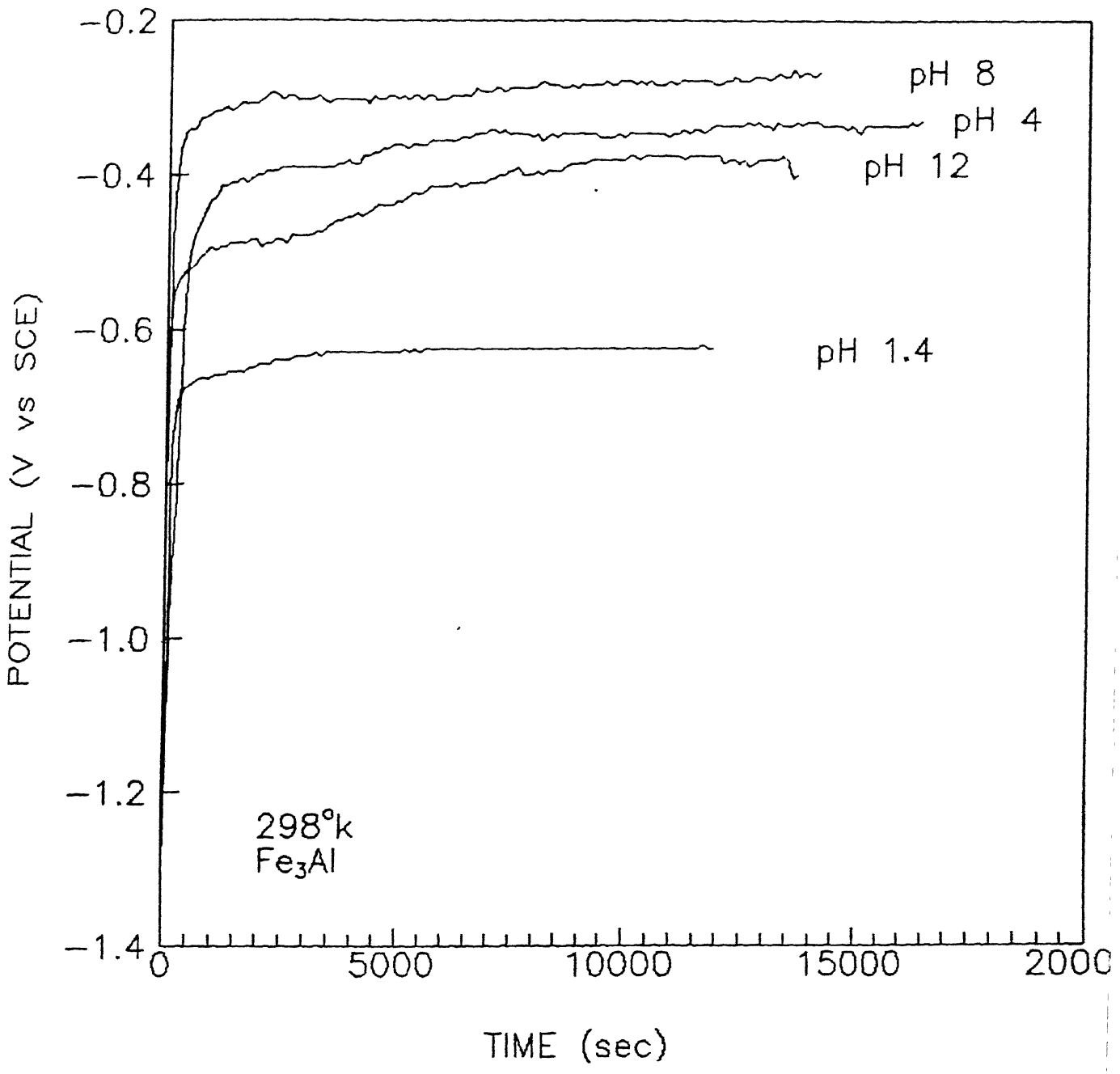

Figure 20 Free corrosion potential as a function of time for Fe_3Al in electrolytes of different pH.

Table 4 Corrosion characteristics of Fe_3Al in electrolytes of different pH

Solution pH	Free corrosion potential (mV vs SCE)	Complete passivation potential (mV vs SCE)	Pitting potential (mV vs SCE)	Passivity range (mV)	Remarks (Behavior)
1.4	-626	——	——	——	Active
4.0	-363	-950	100	1050	Passive
8.0	-272	-750	850	1600	Passive
12	-458	——	1000	——	Passive with cathodic loop

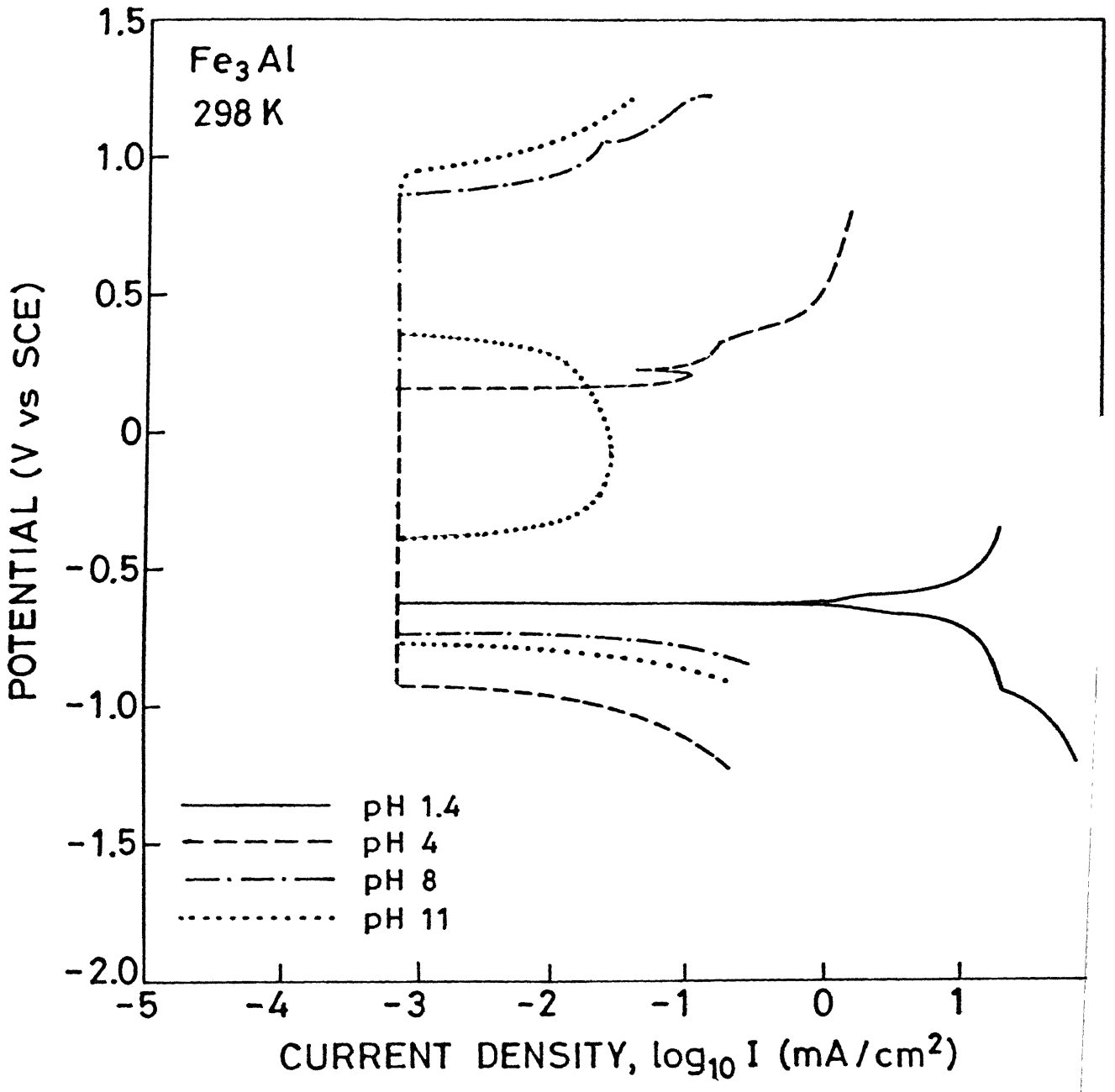

Figure 21 Potentiodynamic polarization curves of Fe_3Al in electrolytes of different pH.

can be explained by first considering the effect of pH on the corrosion behavior of an active-passive alloy. The effect of pH on corrosion of an active-passive alloy can be explained by applying the Nernst equation to the reduction reaction(s). The cathodic reaction could be either hydrogen reduction (equations 13 and 14) for which the electrode potential as a function of pH is given by

$$E = E^{\circ} - 0.059\ pH \qquad E^{\circ} = 0 \text{ vs SHE}$$

or oxygen reduction (equations 15 and 16) for which the electrode potential as function of pH is given by

$$E = E^{\circ} - 0.059\ pH \qquad E^{\circ} = 1.23 \text{ V vs SHE}$$

From these expressions for the electrode potential of reduction reactions, it can be seen that with increase in pH, the electrode potential of the cathodic reaction would shift in the active direction. The anodic polarization curve of the active-passive metals exhibits passivity. The cathodic polarization curve would shift in the active direction by increasing pH because of the shifting of the electrode potential for cathodic reaction in the active direction with increase in pH. As can be seen from Figure 22, pH corresponding to 1.4 should result in experimental polarization curve exhibiting active behavior while that corresponding to pH 4, 8 and 12 should exhibit active-passive behavior. The Evans diagrams based on the mixed potential theory for the case of Fe_3Al corroding electrolyte of different pH are presented in Figure 23. The experimental curve could be obtained by the addition of the theoretical anodic and cathodic polarization curves (Figure 23). As the experimentally observed FCP in electrolyte of pH 8 was noble compared to that in other electrolytes (Figure 20), the anodic polarization curve in electrolyte of pH 8 was assumed to be noble compared to that in other electrolytes. The other

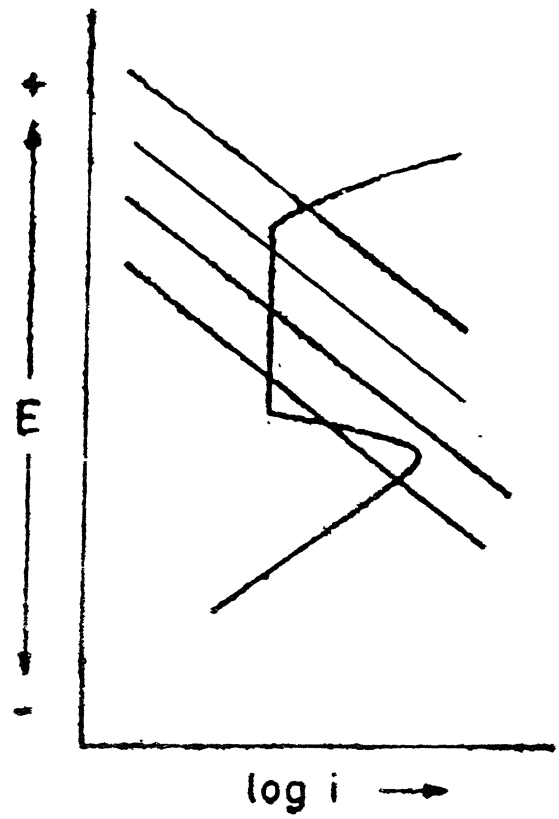

Figure 22 Schematic diagram illustrating the effect of pH on the cathodic polarization curve.

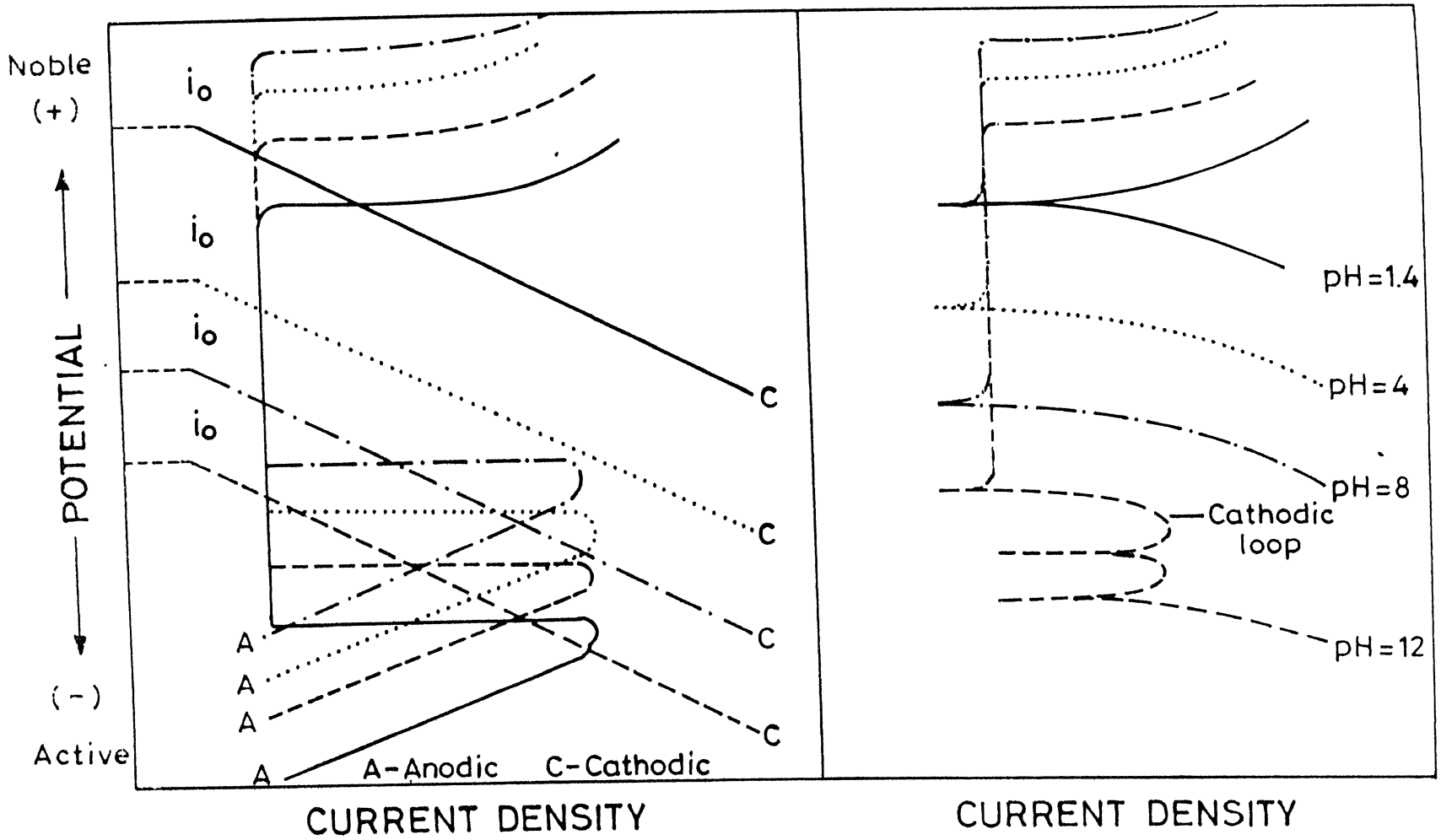

Figure 23 Schematic Evans diagram based on mixed potential theory explaining corrosion behavior of Fe_3Al in electrolytes of different pH.

anodic curves are presented in Figure 23 were similarly constructed according to their relative FCP values. On applying the mixed potential theory by addition of these cathodic and anodic curves in electrolytes of different pH, the experimental polarization curves could be explained.

The corrosion behavior of iron aluminide (FeAl) has been earlier compared to the corrosion behavior of pure iron and aluminium in 1M NaOH and 1N Na_2SO_4 of pH 4, 6 and 10. In the alkaline solution (NaOH), aluminium was preferentially dissolved leaving behind an iron rich surface that lead to passivity, and in the Na_2SO_4 solution, the polarization behavior was more akin to that of Fe. This results suggested that final passive layer on FeAl was an iron oxide/hydroxide that was further validated by X-ray photoelectron spectroscopy study [5]. However the present study dealt with Fe_3Al and passivity of the both Fe and Al could be considered in the following to understand the effect of pH on passivity of Fe_3Al.

The Pourbaix diagram of Al-H_2O and Fe-H_2O system can be used to explain the observed effect of solution pH on passivity. Aluminium is an amphoteric metal for which the protective oxide film dissolves at low and high pH as seen in the Pourbaix diagram (Figure 24). Moreover, Fe also corrodes at low pH while it is passive at high pH. Therefore, in the highly acidic solution the surface oxide was unstable and the intermetallic dissolved. This is reflected in the active behavior of Fe_3Al in the electrolyte of pH 1.4 (Figure 21). However, in the range of intermediate pH 4 to 8, the surface layer was stable and therefore passive behavior was observed for Fe_3Al. In the case of alkaline solution, Fe_3Al exhibited unstable passivity (as indicated by cathodic loop) in electrolyte of pH 12. At this pH, Al_2O_3 is unstable and dissolves as AlO_2^-. This should result

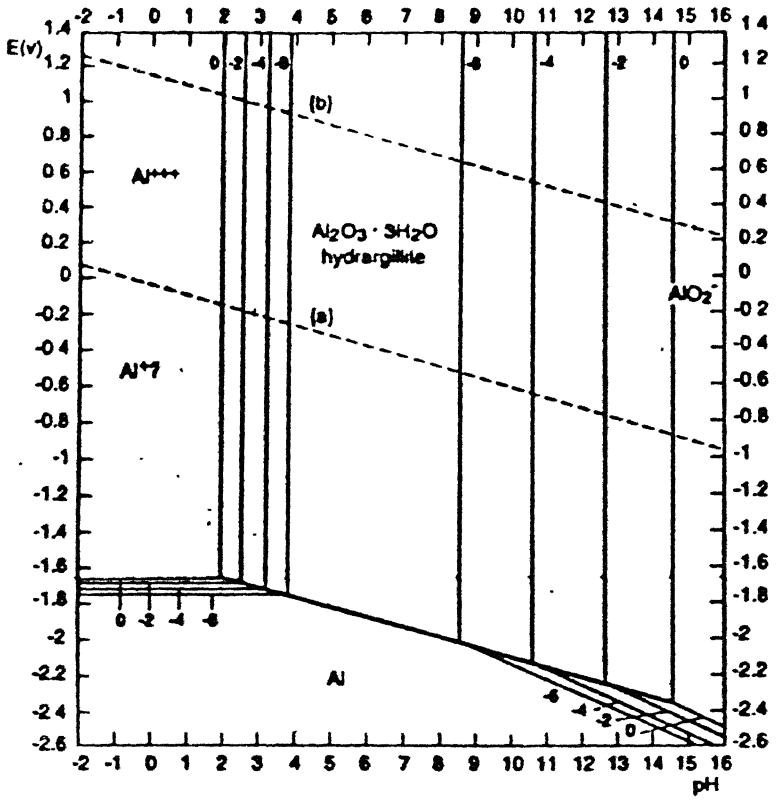

Figure 24 Pourbaix diagram of Al-H_2O system.

in active behavior for Fe_3Al in electrolyte of pH 12. However, the observed unstable passive behavior could be due to the presence of an oxide/surface layer which is not entirely active in the pH range. This passivity could be provided by hydrated Fe oxide. Janavicius and Payer [5] earlier concluded that the passive layer forming on Fe-50Al to be an iron oxide/hydroxide and that its behavior was more directly related to the corrosion behavior of pure iron. It is quite possible that this should be the case with Fe_3Al as the Pourbaix diagram of the $Fe-H_2O$ system (Figure 25) shows that, although the material would be active at low pH, the Fe oxide would passivate at higher pH. Therefore, the study conducted in the electrolyte of different pH indicates that the oxide forming on Fe_3Al under aqueous corrosion condition should contain Fe oxide in it as indicated by the presence of passivity in solution of pH 12.

4.4 COMPARISON OF CORROSION BEHAVIOR OF Fe_3Al WITH STAINLESS STEELS

The potentiodynamic polarization curves of iron aluminide and stainless steels in electrolyte of pH 4 and 8 (without and with Cl^-) are presented in Figure 26 through 29. The corrosion characteristics of iron aluminide and stainless steels in the electrolytes of pH 4 (without Cl^- and with Cl^-) and pH 8 (without and with Cl^-) are listed in Table 5 through 8. The following observations were made from these figures and tables (comparison of Fe_3Al with stainless steel) and these are as follows. The FCP for Fe_3Al is active compared to stainless steel in electrolyte of pH 4 and 8. Iron aluminide exhibited more negative E_{cp} compared to stainless steels, indicating easy passivation for iron aluminide. It exhibited noble pitting potential compared to stainless steel in the electrolyte of pH 8. However, reverse was the case in the electrolyte of pH 4 where it exhibited

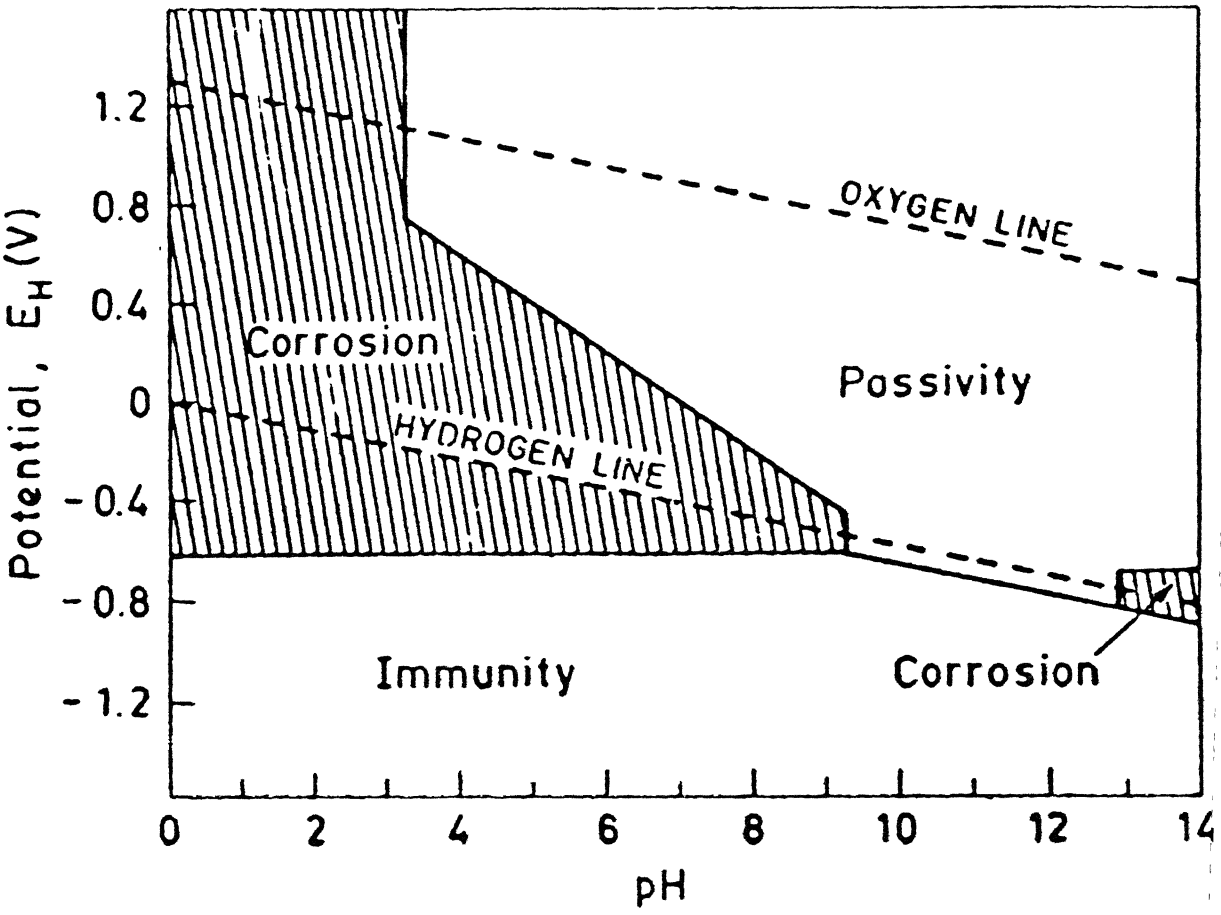

Figure 25 Pourbaix diagram of Fe-H_2O system.

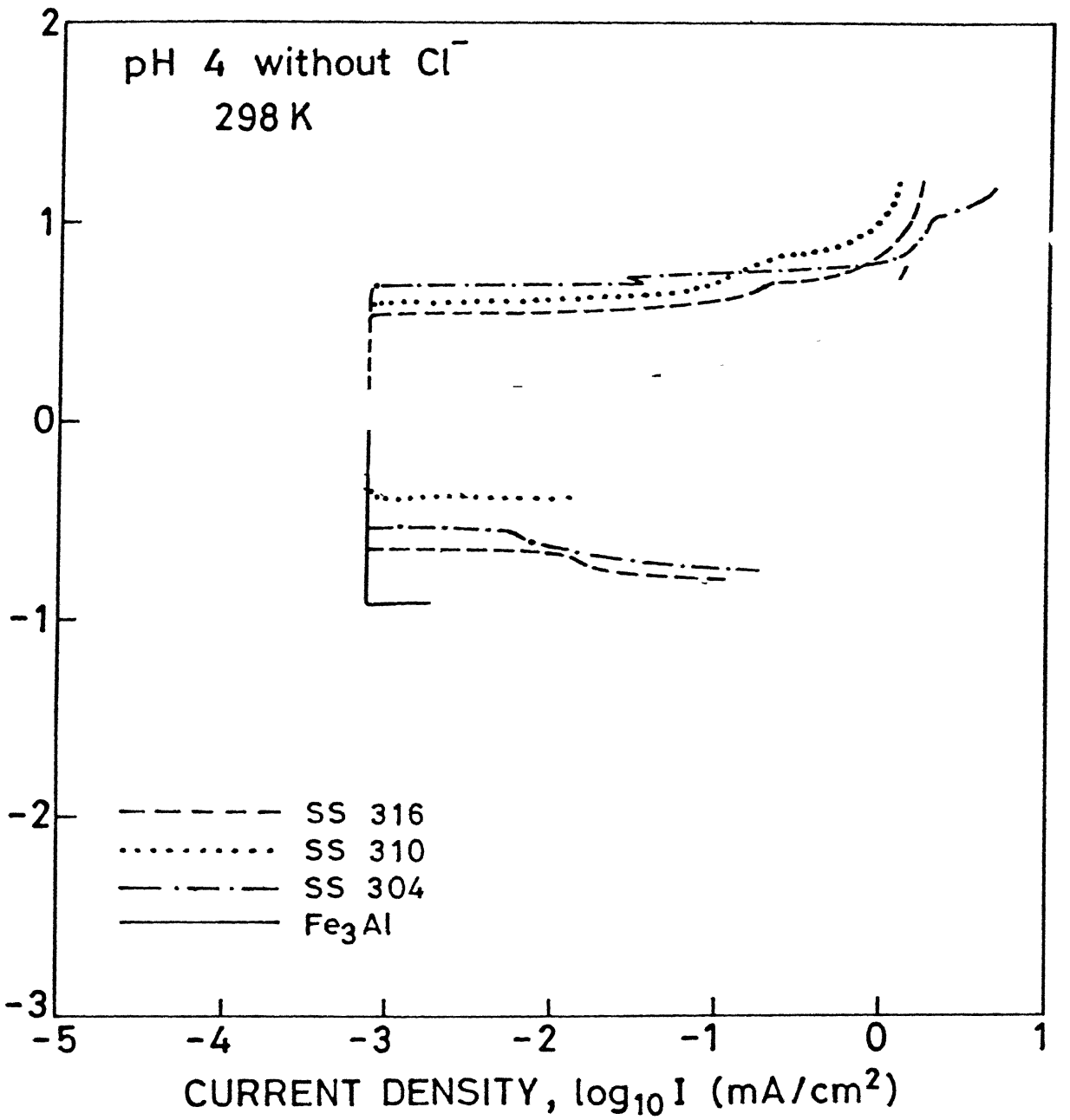

igure 26 Potentiodynamic polarization curves of Fe_3Al and stainless steels in H_2SO_4 electrolyte of pH 4 without chloride ion.

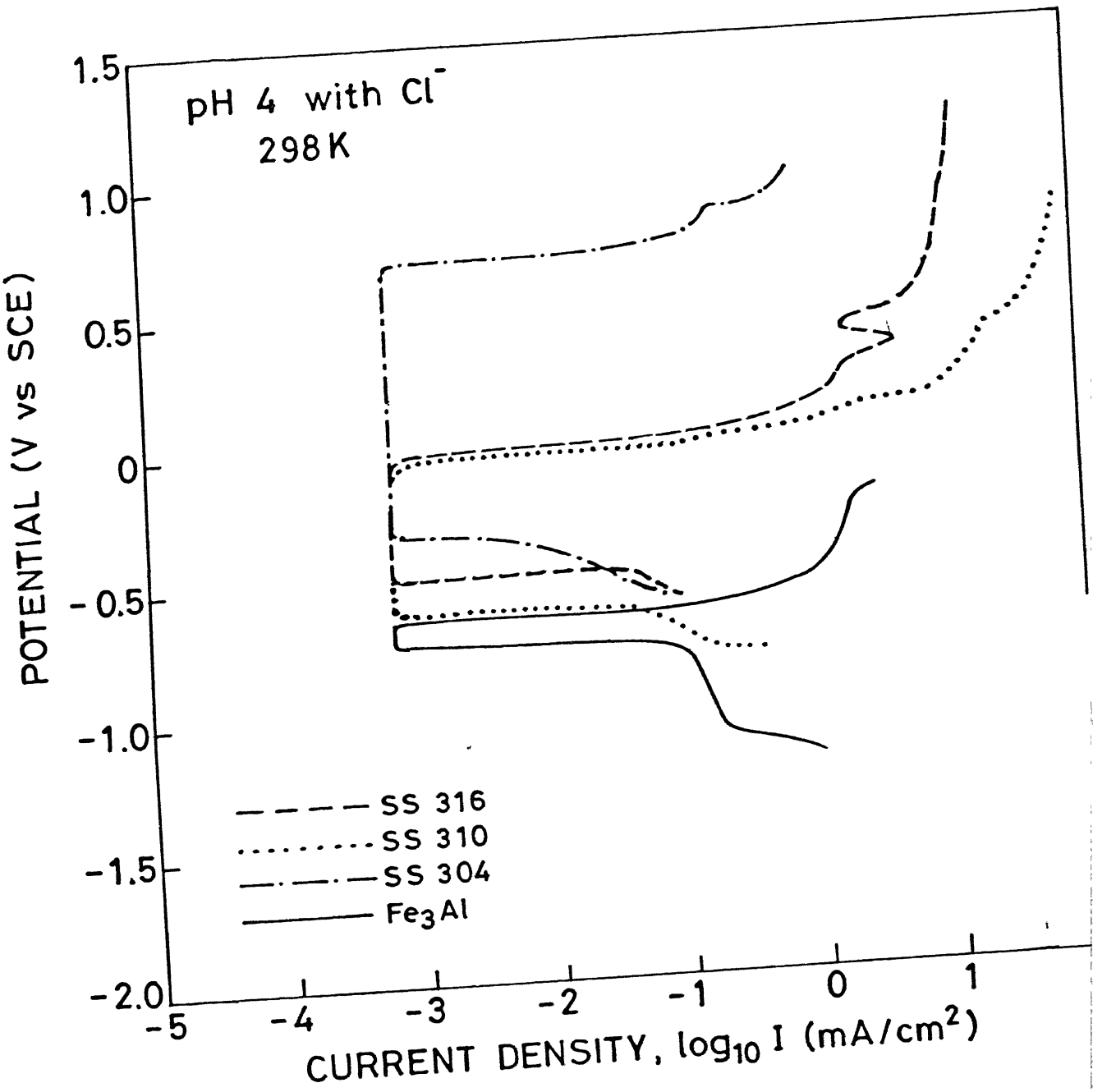

Figure 2 Potentiodynamic polarization curves of Fe_3Al and stainless steels in H_2SO_4 electrolyte of pH 4 with chloride ion.

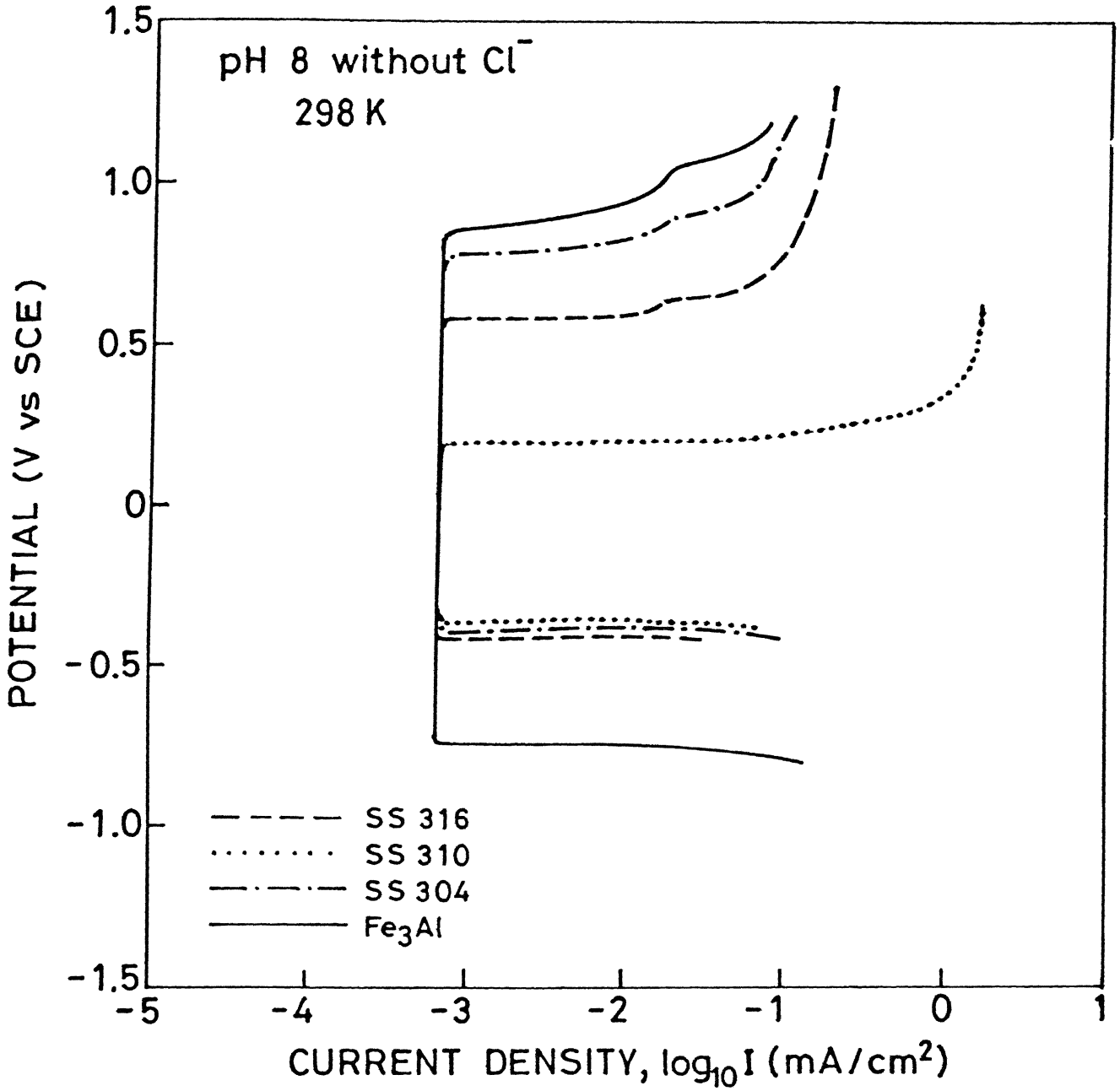

Figure 28 Potentiodynamic polarization curves of Fe_3Al and stainless steels in H_2SO_4 electrolyte of pH 8 without chloride ion.

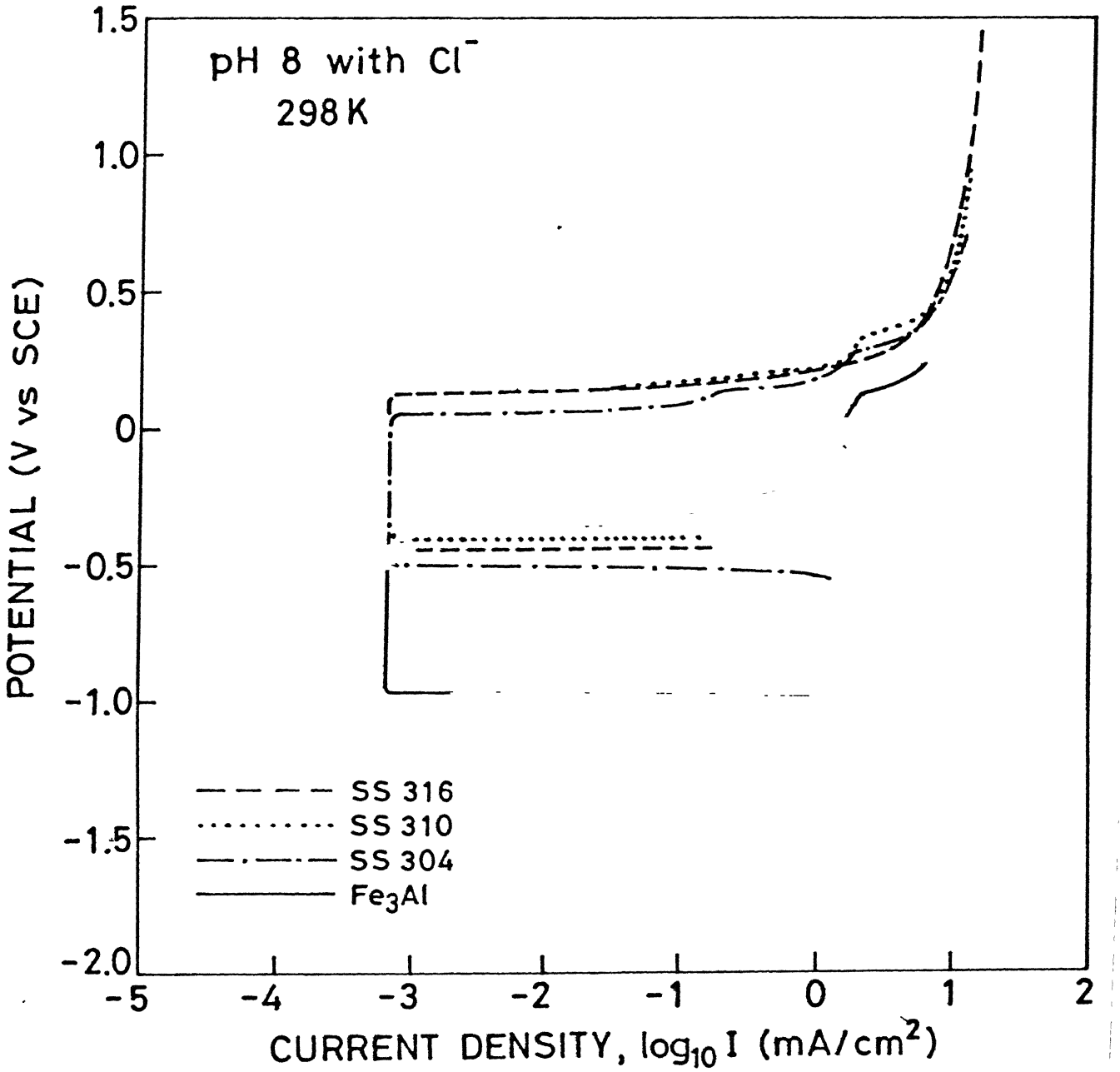

Figure 4 Potentiodynamic polarization curves of Fe_3Al and stainless steels in H_2SO_4 electrolyte of pH 8 with chloride ion.

Table 5 Corrosion characteritstics of stainless steels 304, 310, 316 and iron aluminide in electrolyte of pH 4 without Cl^-

Sample	Free corrosion potential (mV vs SCE)	Complete passivation potential (mV vs SCE)	Pitting potential (mV vs SCE)	Passivity range (mV)
Fe_3Al	-322	-950	100	1050
SS 304	-180	-600	650	1250
SS 310	-58	-450	575	1025
SS 316	-135	-650	500	1150

Table 6 Corrosion characteristics of stainless steel 304, 310, 316 and Fe_3Al in electroplyte of pH 8 without Cl^-

Sample	Free corrosion potential (mV vs SCE)	Complete passivation potential (mV vs SCE)	Pitting potential (mV vs SCE)	Passivity range (mV)
Fe_3Al	-272	-750	850	1600
SS 304	-78	-410	775	1185
SS 310	-68	-375	200	575
SS 316	-78	-425	575	1000

Table 7 Corrosion characteristics of stainless steel 304, 310, 316 and Fe_3Al in electroplyte of pH 4 with 200 ppm Cl^-

Sample	Free corrosion potential (mV vs SCE)	Complete passivation potential (mV vs SCE)	Pitting potential (mV vs SCE)	Passivity range (mV)
Fe_3Al	-668	-750	-650	100
SS 304	-151	-300	700	1000
SS 310	-131	-700	-25	675
SS 316	-144	-500	-25	475

Table 8 Corrosion characteristics of stainless steel 304, 310, 316 and Fe_3Al in electroplyte of pH 8 with Cl^-

Sample	Free corrosion potential (mV vs SCE)	Complete passivation potential (mV vs SCE)	Pitting potential (mV vs SCE)	Passivity range (mV)
Fe_3Al	-464	-869	-395	474
SS 304	-130	-500	50	550
SS 310	-81	-425	140	565
SS 316	-140	-450	140	590

active pitting potential compared to stainless steel. Chloride induced pitting resistance was very poor for iron aluminide compared to stainless steels, indicating more detrimental effect of chloride ion in the electrolyte to the passive layer formed on Fe_3Al. Therefore, the passivity range of iron aluminide in the electrolyte having chloride ion was shorter compared to stainless steel.

It is seen from the Pourbaix diagrams of Al/H_2O (Figure 24) and Fe/H_2O (Figure 25), the stability of the passive film on Fe increases with increasing pH. However, the range of passivity of Cr_2O_3 film does not change with pH (Figure 30). Therefore, iron aluminide could have exhibited better passivity compared to stainless steel in electrolyte of pH 8.

For the case of stainless steels chromium oxide would be the film which give passive layer. For this case Cl^- incorporation in the solution does not cause any change in film thickness or any thinning or breakdown of film. However, the susceptibility of the passive film to Cl^- attacks appears to depend on the presence of small amount of impurity in the alloy [13]. In the case of iron aluminide, Chloride ions would have been detrimental to the iron oxide/hydroxide passive layer. One interpretation of the result of chloride ions is that the ions preferentially get adsorbed at film inhomogeneities and defect sites [14]. This adsorption would be potential dependent and, since a critical concentration of chloride ion is thought to be required for breakdown, significance of the pitting potential becomes evident. It has also been suggested that adsorption of chloride ions on the passive film surface lowers the interfacial tension at the film/solution interface, causing the formation of cracks [15] or increasing the electrostiction pressure above a critical value to bring about breakdown [16]. Another view is that two-dimensional nuclei of halide salt

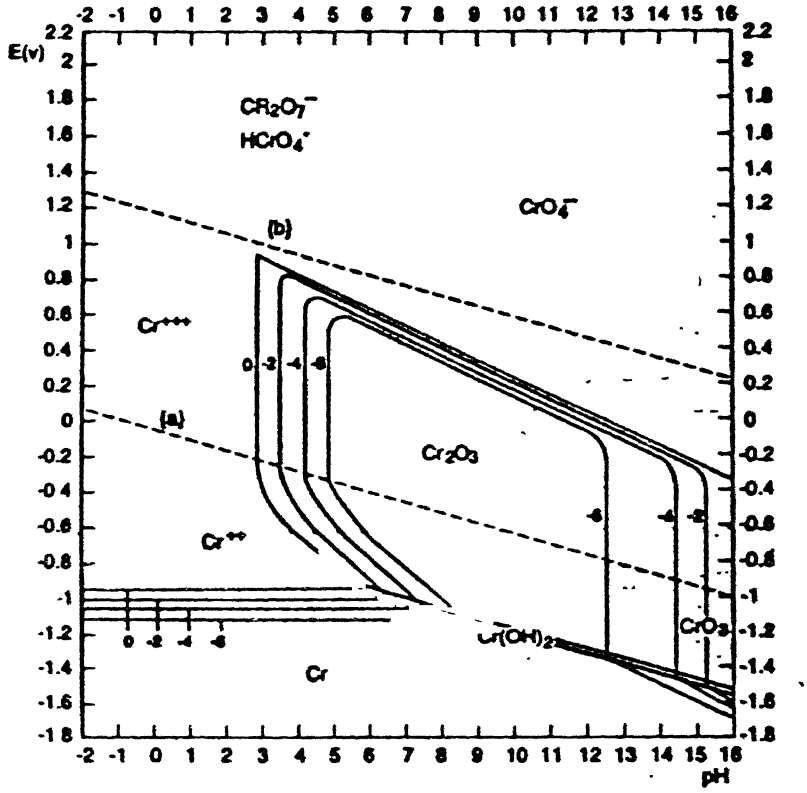

Figure 30 Pourbaix diagram of Cr-H_2O system.

layers form locally and give rise to thinning (by way of chemical dissolution) and eventually local removal of passive film [17]. Others have suggested that chloride ion incorporation into the passive oxide film lattice is precursor to film breakdown and pit initiation. Incorporation can be either by ionic migration under an electric field or field independent anion exchange [18-20]. The incorporated chloride ions may enhance metal cation diffusion to the surface and thereby generate cation vacancies at the metal/film interface [21]. If the rate of vacancy formation is sufficiently high, voids formation may cause a local collapse of the passive film. Another theory involves the supposition that passive films are wet and that the incorporated chloride ions displace from the lattice water molecules, which are essential for passivity [22-24]. A somewhat different approach to the theory of film breakdown suggests that the role of aggressive chloride ions in pit initiation is not necessarily to thin, break or incorporate into the passive film prior to breakdown, but rather to simply interfere with reformation of the film. The film is believed to be continuously breaking down and reforming at local defects sites [25-26] and therefore the ability of the halide ion to hinder repassivation is the key to local film breakdown. If Al_2O_3 had been the passivating layer on Fe_3Al, chloride ions would have detrimental effect on the pitting behavior. This is for the following reason. Pitting was found most commonly in aluminium corrosion resulting the failure of passive alumina (Al_2O_3) layer [27]. In a near neutral aqueous solution (pH < 7) where local cell action is sufficiently vigorous to disturb the homogeneity of the solution and build up local acidity, alumina is no longer able to form a protective film close to the metal. When the aluminium ions migrate from the areas of low pH, alumina precipitates as membrane, further

isolating and intensifying local acidity, and pitting of the metal results. However, the near neutral aqueous solution (pH > 7), high passivity range and more negative E_{cp} dominated and local cell action would have been no longer able to build up acidity, and therefore the alumina layer would have been stable that the pitting potential was high compared to stainless steel in electrolyte of pH 8. Chloride ions, which have been thought to be able to penetrate into aluminium oxide films, can be particularly harmful for the underlying aluminium metal [28-36]. It has been interpreted that after the film breakdown, bare aluminium surface sites are exposed to the electrolyte and consequently, the metal dissolution takes place [37-38]. It is well known that pitting process of aluminium in chloride solutions takes place as crystallographic etching at low anodic potentials, while at higher anodic potentials polished hemispherical pits appear [39-40]. Chloride ions are more damaging to Al_2O_3 because they attack the film only at weak spots [10]. The sign of surface charge effects the subsequent adsorption of ions present in the solution. In solutions of pH < 9, the oxide surface is positively charged and chlorides are likely to be adsorbed. Preferential adsorption at weak spot in the passive film is responsible for the localization of corrosion attack [41]. Therefore chloride ions are detrimental even if Fe_3Al contains oxides of aluminium on its surface.

The following observation could be made on the corrosion behavior of stainless steels. The FCP for 310 was noble compared to 316 in electrolyte of pH 4 and 8 (without and with Cl^-). The FCP stabilized when the film of Cr_2O_3 either covered entire surface or increased from minimum required thickness on the stainless steel. Nickel is austenitic stabilizer by stabilizing the FCC structure and provides additional corrosion

resistance. Therefore, the high Cr and Ni contents in 310 (compared to 316) could have stabilized FCP at a noble value compared to 316.

The E_{pit} for 310 and 316 were same in electrolyte of pH 4 and 8 containing Cl^-. However, E_{pit} was comparable for 310 and 316 in electrolyte of pH 4 (without Cl^-) and E_{pit} was higher for 316 compared to 310 in electrolyte of pH 8 (without Cl^-). Mo is added to stainless steels for pitting resistance [10]. Mo enhanced pitting resistance in 316 in the electrolyte containing Cl^-. High Ni (19%) and Cr (25%) combination also enhanced similar pitting resistance in 310. Therefore similar E_{pit} was observed for both the stainless steels in electrolyte containing Cl^-. In fact the effect of Mo along with Fe-Ni-Cr offer reliable performance in oxidizing as well as reducing media [42] and it could even surpass the pitting resistance effect of high Cr-Ni iron alloys in slightly alkaline solutions. Therefore higher E_{pit} was observed for 316 compared to 310 in the electrolyte of pH 8.

The passivity range was larger for 316 compared to 310 in electrolytes of pH 4 and 8 (without Cl^-). However, the passivity range was comparable in both the electrolyte containing Cl^-. Mo offers excellent resistance along with Fe-Ni-Cr in oxidizing and reducing media. This could be the reason for higher passivity range of 316 compared to 310 in both the electrolyte. However, chloride ions in the electrolyte affect the pitting and reduce the passivity range. Therefore, the passivity range was comparable for 310 and 316 in electrolytes of pH 4 and 8 containing chloride ions.

The E_{cp} was comparable for 310 and 316 in electrolytes of pH 4 and 8 both (both without and with Cl^-). It has been earlier observed that passivation in stainless steels was comparable if they contained Cr > 12.7%

in the slightly alkaline electrolyte [43]. This could be the reason of comparable E_{cp} for 310 and 316 in the electrolyte of pH 8 (both without and with Cl^-).

The behavior of 304 was anomalous compared to others as it showed high pitting potential compared to 316 (although it did not contain Mo) and larger passivity range than 316 & 310. The reason may be the 304 was obtained from one source (commercially available less reliable supplier) while 316 and 310 were obtained from reliable source. The composition of commercially available 304 did not match with the AISI specification whereas the corrosion behavior of 316 and 310 were comparable to AISI specifications.

4.5 CORROSION BEHAVIOR OF Fe_3Al-5M (M = Cr, Mo, Ta and Ti) INTERMETALLICS

The potentiodynamic polarization curves of Fe_3Al-5M (M = Cr, Mo, Ta and Ti)intermetallics in electrolyte of pH 4 and 8 are presented in Figure 31 and 32 , respectively. The corrosion characteristics of Fe_3Al-5M and binary Fe_3Al in electrolyte of pH 4 and 8 are summarized in Table 9 and 10. The following comparative observations could be made for Fe_3Al-5M intermetallics and binary Fe_3Al. The complete passivation potential (E_{cp}) were more negative for Fe_3Al-5M intermetallics compared to binary Fe_3Al, thereby indicating that it should be easier to passivate Fe_3Al-5M compared to Fe_3Al. The pitting potentials (E_{pit}) were noble for Fe_3Al-5M intermetallics compared to binary Fe_3Al thereby indicating that they show passivity to much higher potential without pitting compared to binary Fe_3Al, in the electrolyte of pH 4. However the reverse was the case in electrolyte of pH 8, where Fe_3Al showed noble pitting potential compared to Fe_3Al-5M intermetallics. The passivity range was larger for Fe_3Al-5M

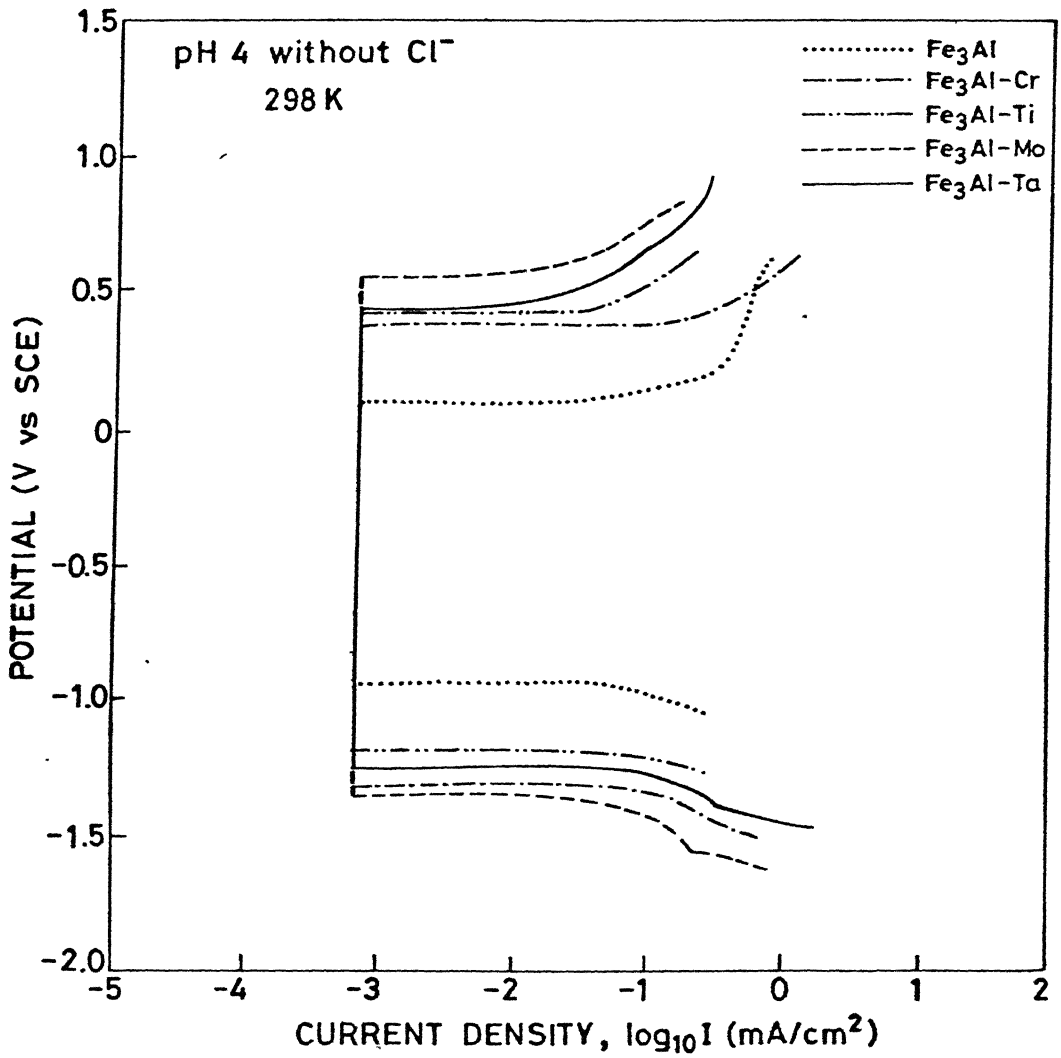

Fig. 31 Corrosion characterstics of Fe_3Al-5M and binary Fe_3Al in the electrolyte of pH 4 without Cl^-.

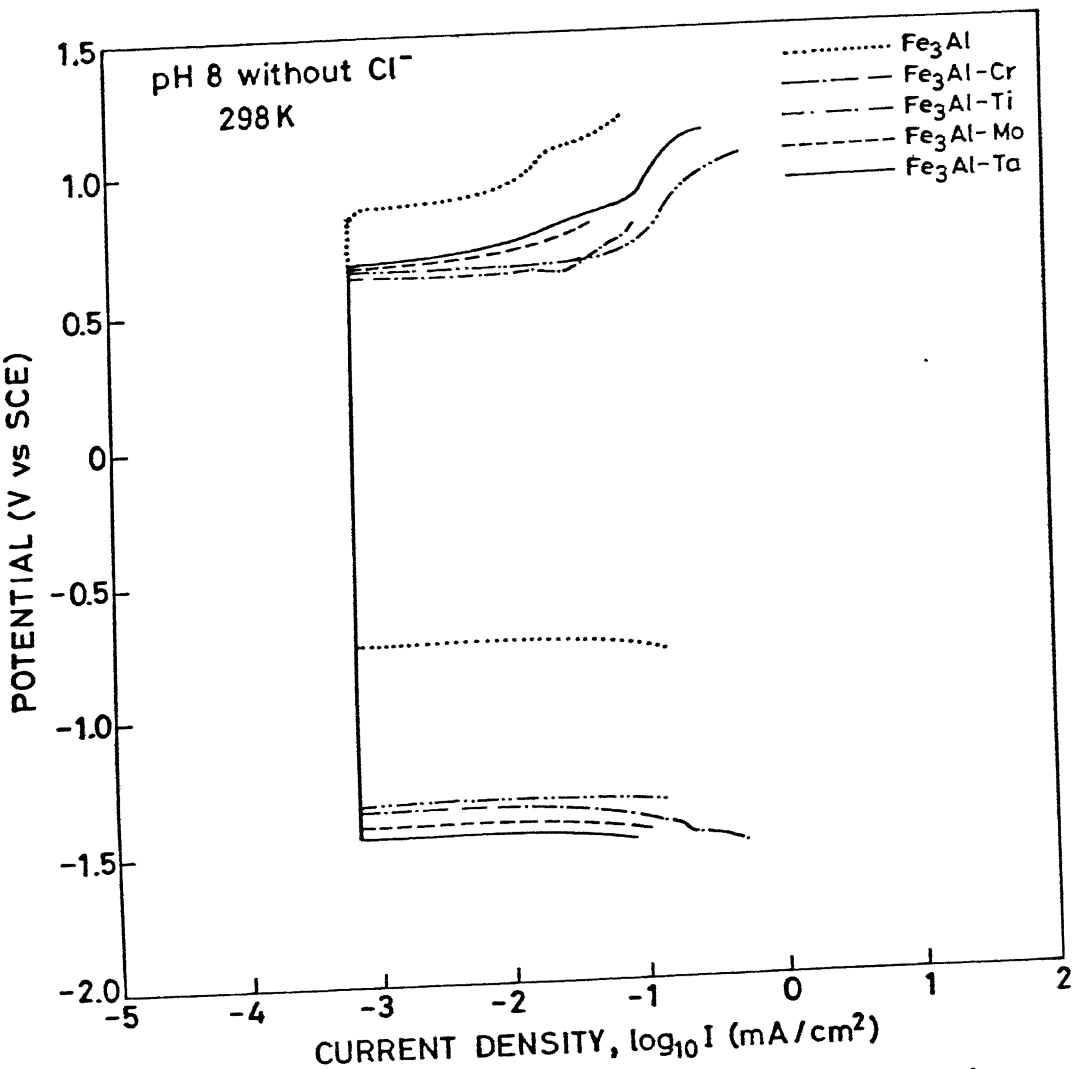

Fig. 32 Corrosion characteristics of Fe_3Al-5M and binary Fe_3Al in the electrolyte of pH 8 without Cl^-.

Table 1 Corrosion characteristics of Fe_3Al-5M and binary Fe_3Al in electroplyte of pH 4

Sample	Free corrosion potential (mV vs SCE)	Complete passivation potential (mV vs SCE)	Pitting potential (mV vs SCE)	Passivity range (mV)
Fe_3Al	-363	-950	100	1050
Fe_3Al-Cr	-330	-1333	400	1733
Fe_3Al-Ti	-350	-1196	444	1640
Fe_3Al-Mo	-334	-1360	585	1945
Fe_3Al-Ta	-293	-1264	454	1718

Table 2 Corrosion characteristics of Fe_3Al-5M and Fe_3Al in electroplyte of pH 8

Sample	Free corrosion potential (mV vs SCE)	Complete passivation potential (mV vs SCE)	Pitting potential (mV vs SCE)	Passivity range (mV)
Fe_3Al	-272	-750	850	1600
Fe_3Al-Cr	-180	-1381	634	2015
Fe_3Al-Ti	-180	-1357	664	2021
Fe_3Al-Mo	-187	-1435	690	2125
Fe_3Al-Ta	-141	-1480	700	2180

intermetallic compared to binary Fe_3Al in electrolytes of pH 4 and 8. The FCP of Fe_3Al-5M intermetallics was noble compared to binary Fe_3Al in both the electrolytes (pH 4 and 8). The above observations could be explained as follows.

Introducing a new component that passivates easily into a metal or alloy causes the metal or alloy to take on, to a greater or lesser extent, the passive properties of the introduced material [43]. The proposed explanation for the effect of such alloying elements and mechanism of their action can be thus deduced to the following reasons. Firstly, the emergence of the surface planes of stable (passive) atoms due to the formation in the alloy of ordered structures of the alloying component would result in enhanced passive behavior [44-45]. Moreover, gradual enrichment by the corrosion process in the surface layer of a solid metallic solution with atoms of more stable/passive component would also be helpful [46-48]. An increase in the concentration of the more stable component of the alloy results in the formation of new surface structures, such as intermetallic compounds, or even a surface layer of the stable component, and confers additional passivity. Secondly a change in the internal structure of the atoms through the formation of solid solutions could result in enhanced passivity [49-54]. The E_{pit} of binary iron aluminide in electrolyte of pH 8 was very high (noble) due to favorable stable protective surface layer, as discussed earlier. Therefore, further alloying by passive element did not have any effect on the E_{pit}, although they did help in enhancing the passivity range and shifting the E_{cp} in active direction.

The following comparative observations could be made for Fe_3Al-5M intermetallics. Fe_3Al-5Ta had excellent corrosion resistance in

electrolyte of pH 8, as it exhibited better corrosion characteristics (noble E_{pit}, noble FCP, active E_{cp} and larger passivity range) compared to others. The FCP of Fe_3Al-5Ta was noble in both electrolyte of pH 4 and 8 compared to others. All the other intermetallic exhibited comparable FCP in both electrolytes. The E_{cp} for Fe_3Al-5Cr and Fe_3Al-5Mo were more negative compared to other intermetallics in the electrolyte of pH 4, thereby indicating that it should be easier to passivate Fe_3Al-5Cr and Fe_3Al-5Mo intermetallics compared to other in this electrolyte. The E_{pit} for Fe_3Al-5Mo intermetallic was noble compared to other intermetallic in electrolyte of pH 4. The corrosion behavior of Fe_3Al-5Cr and Fe_3Al-5Ti intermetallics were comparable in electrolyte of pH 8. They exhibited poor corrosion behavior (lower E_{pit} lower passive range) compared to others in electrolytes of pH 4 and 8.

Effect of Tatalum

Tantalum metal has excellent corrosion resistance to most acids as well as to most aqueous salt solutions and organic chemicals. For example, in aqueous solution of NaOH (10 %), at room temperature, it exhibits a very low (0.00025 mm/y) corrosion rate [27]. Tantalum would have been enriched on the Fe_3Al-5Ta surface as X-ray diffraction analysis of Fe_3Al-5Ta showed the existence of two other metallics, which verified the existence of other ordered phases. However, XRD did not indicate presence of new phase in other intermetallics as seen in the diffraction pattern Figure 33. This argument could explain the better corrosion behavior of Fe_3Al-5Ta intermetallic compared to others.

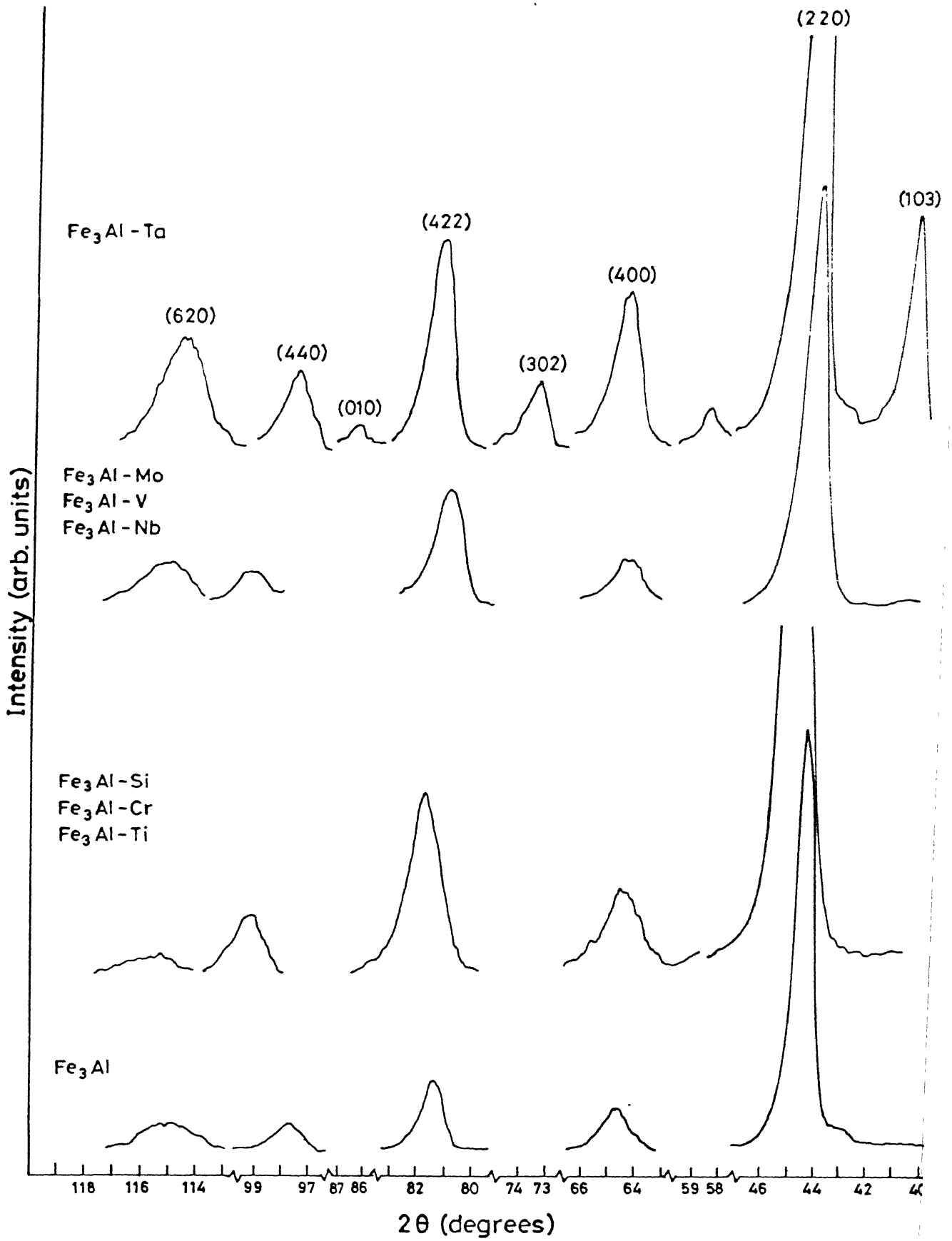

Figure 33 XRD patterns of Fe_3Al-5M intermetallics.

Effect of Chromium and Molybdenum

In iron based alloys containing chromium or other passive alloying element like Mo and Si, the corrosion resistance is contingent on its ability to passivate [43]. Chromium and molybdenum are placed in same group and having same crystal structure (BCC), they could possibly change the internal structure of iron aluminide atoms through the formation of solid solutions. For instance it is considered that five vacancies in the chromium atom in the 3d electron level make it possible for each chromium atom to share five electrons from iron and transfer five iron atoms into the passive state. This could be one of the reason for the better passivation of Fe_3Al-5Cr and Fe_3Al-5Mo.

Effect of Molybdenum

Molybdenum has excellent corrosion resistance to mineral acids. It is not attacked by iodine vapor, bromine and chlorine up to slightly high temperature [42]. Small amount of Mo enhanced the pitting potential of Fe_3Al as it was observed earlier [12]. This could be the explanation of higher pitting potential of Fe_3Al-5Mo.

Effect of Titanium and Chromium

Titanium is a highly reactive metal, forming a continuous stable, protective and adherent oxide film on the surface in the presence of oxygen and moisture. The TiO_2 film is formed in all pH, and titanium alloys are predictably resistant to a host of normally aggressive alkaline and acid media. But corrosion resistance is generally unaffected by low level of its addition as alloying element [12]. Same effect was found with small addition of Cr. Alloy with 12% or more Cr gives better corrosion

resistance. This could be explanation of poor corrosion behavior of Fe_3Al-5Cr and Fe_3Al-5Ti compared to others in both the electrolytes, as Ti and Cr additions were up to only 5 at % each.

CHAPTER 5

CONCLUSIONS

5.1 CONCLUDING REMARKS

Based on the work presented herein, the following concluding remarks were made.

1. A scan rate of 1 mV/sec was found ideal for potentiodynamic polarization study, as scan rates above 1 mV/sec provided active zero current potentials. The surface conditions were stable below this scan rate as the as ZCP was the same for scan rates below 1 mV/sec.
2. The corrosion rate of Fe_3Al was minimum in naturally aerated solution compared to aerated/deaerated solution. Moreover, Fe_3Al exhibited larger passivity range in naturally aerated compared to aerated in electrolyte of pH 4.
3. Low oxygen environments did not favour the formation of protective oxide films in stainless steel whereas it aided passive film formation in the case of iron aluminide.
4. Iron aluminide exhibited passive behavior in electrolyte of pH 4, 8 and 12. However, it exhibited active behavior in electrolyte of pH 1.4. Moreover, in electrolyte of pH 12, it exhibited unstable passivity. The passivity range was larger in electrolyte of pH 8 than that of pH 4. The polarization behavior in electrolyte of different pH has been explained by considering Evans diagram based on mixed potential theory.
5. The corrosion behavior of Fe_3Al was found to be better than stainless steel in electrolyte of pH 8. However, they showed comparable corrosion behavior in electrolyte of pH 4.

6. Corrosion characteristics of Fe_3Al were better in electrolyte of pH 8 than that of pH 4. The possible reason have been elucidated by considering the Pourbaix diagram of Fe-H_2O and Al-H_2O.
7. Chloride induced pitting resistance of stainless steel was better compared to iron aluminide, as chloride ions lead to a greater deterioration of passivation behavior and pitting resistance of Fe_3Al compared to stainless steel.
8. The corrosion behavior of Fe_3Al-5M (M = Cr, Ti, Mo and Ta) was better in electrolytes of pH 4 and 8 compared to binary Fe_3Al, as alloying element M, induced additional passivity to the intermetallic Fe_3Al-5M. possible reasons for the effect of alloying addition have been discusses

5.2. SCOPE FOR FUTURE WORK

1. Effect of temperature on the corrosion behavior of iron aluminide could be studied. As it is well known that an increase in temperature impairs passivity of stainless steel, it would be interesting to see the effect on Fe_3Al.
2. Electrolyte of pH ranging between 1.4 - 4, and 8 - 12 could be utilized for corrosion experiments to elucidate the nature of passive layers forming on the iron aluminide.
3. Surface analysis using technique like Auger Electron Spectroscopy (AES) and X-ray Photoelectron Spectroscopy (XPS) could be used to characterize dissolution behavior of pits and nature of the passive protective oxide on iron aluminide.
4. Fe_3Al-5M type intermetallics could be prepared with different amounts of alloying elements to study their effect on corrosion behavior.

5. Some intermetallics of type Fe_3Al-M-N could be made in order to find proper compositions for much better corrosion behavior, as it was found earlier that both high Cr levels (4-6 at%) and Mo additions (1-2 at%) were desirable for satisfactory resistance to chloride induced localized corrosion.

6. Cyclic anodic polarization test could be done to reveal the break down potential for pitting corrosion of binary Fe_3Al and Fe_3Al-5M intermetallic in electrolyte of pH 8 with chloride.

REFERENCES

1. C.T.Liu and K.S. Kumar, "Ordered intermetallic alloys, part 1: Nickel and iron aluminides", J. Metals, 45, 38-44 (1993).
2. V.K.Sikka, S.Viswanathan and C.G. Mckaney, "Development and commercialization status of Fe_3Al-based intermetallic alloys", Structured intermetallics, Eds. R. Darolia, J.J.Kewandoski, C.T. Liu, P.L. Martin and M.B. Nathal, TMS, Warrendale, USA, 483-491 (1993).
3. K.Oki, M.Hasaka and T.Eguchi "Process of order-disorder transformation in iron-aluminium alloys", Japanese J. of Appl. Phys., 12, 1522-1530 (1973).
4. H.Okamoto and P.A.Beck, "Phase relationships in the iron rich Fe-Al alloys, Met. Trans. A, 2, 569-574 (1971).
5. P.V.Janavicius and J.H.Payer, "Environmental Effects on Advanced Materials, Eds. R.H. Jones and E.Ricker, TMS, Warrendale, USA, 199-212 (1991).
6. R.A.Buchanan and J.G.Kim, "High temperature ordered intermetallic alloys IV, Mat. Res. Soc.Symp. Proc., 213, Eds., L.A.Jones, D.P.Pope and J.O.Stiegler, MRS, Pittsburgh, USA 945-951 (1991).
7. R.Narayan, "An introduction to metallic corrosion and its prevention, Oxford and IBH Publishing Co., New Delhi.
8. J.Jankowski and R. Juchniewicz, "A four-point method for corrosion rate Determination", Corr. Sci., 20, 841-851 (1980).
9. K.Kanno, M.Suzuki and Y.Sato, "Tafel slope determination of corrosion reaction by coulostatic method", Corr. Sc., 20, 1059-1066 (1980).

10. S.A.Bradford, "Corrosion Control", Van Nostrand Reinhold, New York, USA, 16-17, 178-179, 193, 198 (1993).

11. Standard Practice for Laboratory Immersion, Corrosion testing of metals , G 31-72, "Annual Book of ASTM Standard", ASTM, Philadelphia, USA, 03.02, 102 (1991).

12. D.A.Jones, "Principles and prevention of corrosion", Maxwell Macmillan International Publishing Group, New York, USA, 117, 210, 522-524 (1992).

13. V.Mitrovic-Seepanovic, B.Macdougall and M.J. Graham, Corr. Sci., 27, 239 (1987).

14. H.H.Strehblow and B.Titze, "Pitting potentials and inhibition potentials of iron and nickel for different aggressive and inhibiting anions" Corr. Sci., 17, 461 (1977).

15. T.P.Hoar, "The production and breakdown of the passivity of metals", Corr. Sci., 7, 355, (1967).

16. N.Sato, "Anodic breakdown of passive films on metals", J. Electrochem. Sco., 129, 255-260, (1982).

17. K.E.Heusler and L.Fischer, Werkst, Korros, 27, 551, (1976), 27, 697, (1967), 27, 788, (1976).

18. J.Kruger "Passivity and its breakdown on iron and iron based alloys", Eds. R.W.Staechle and H.Okada, NACE, Houston, 91, (1976).

19. H.H.Strehblow, Werkst. Corros, 27, 792, (1976).

20. C.L.Mcbee and J.Kruger, Proc. of U.R. Evans. Inst. Conference on Localized Corrosion, 1971, NACE Houston, 252, (1974).

21. C.Y.Chao, L.F.Lin and D.D.Macdonald, "A point defect model for anodic passive films" J. Electrochem. Soc., 128, 1187-1194, (1981).

22. G.Okamoto, "Passive film of 18-8 stainless steel structure and its functions", Corr. Sci., 13, 471-489, (1973).

23. R.W.Revie, B.G.Baker and J.O'M.Bockris, "The passive film on iron: An application of auger electron spectroscopy". J. Electrochem. Soc., 122, 1460-1466, (1975).

24. W.E.O'Grady, "Mossbauer study of the passive oxide film on iron", J. Electrochem. Soc., 127, 555-563, (1980).

25. B.Mocdougall, "Effect of Cl^- on the localized breakdwon of nickel oxide films, J. Electrochem. Soc., 126, 919-925, (1979).

26. B.Macdougall and M.J.Graham, "Influence of incorporated Cl^- in NiO on the pitting susceptibility of nickel", J. Electrochem. Soc., 131, 727-730, (1984).

27. L.L.Shrier, "Corrosion", Vol. 1, Newenes-Butterworths, London, 4.11, 5.67, (1965).

28. A.R.Despic, D.M.Drazic and L.J.Gajic-Krstazic, J. Electronal. Chem., 242, 303, (1988).

29. I.L.Rozenfel'd, V.P.Persiantsiva and V.E. Zorina, Prot. Met., (USSR), 15, 69, (1979).

30. T.H.Nguyen and R.T.Folely, "The chemical nature of aluminium corrosion", J. Electrochem. Soc., 129, 27-32, (1982).

31. T.R.Beck, Electrochem. Acta, 29, 485, (1984).

32. S.Sato, Y.Itoi and A. Hasumi, Electrochem. Acta, 26, 1303, (1981).

33. Lj.D.Atanasoska, D.M.Drazic, A.R.Despic and A.Zalar, J. Electronal Chem. 182, 179, (1985).

34. T.Hagyard and W.B.Earl, "Potential of aluminium in aqueous chloride solution", J. Electrochem. Soc., 114, 694-698, (1967).

35. T.Hagyard and J.R.Williams, "Potential of aluminium in aqueous chloride solutions Part 1", Trans. Faraday Soc., 57, 2288-2294, (1961).

36. T.Hagyard and M.J.Prior, "Potential of aluminium in aqueous chloride solutions Part 2", Trans. Faraday Soc., 57, 2295-2298, (1961).

37. T.H. Naguyen and R.T.Foley, "On the mechanims of aluminium", J. Electrochem. Soc., 126, 1855-1860, (1979).

38. F.B.Ford, G.T.Burstein and T.P.Holar, "Bare surface reaction rates and their relation to environment controlled cracking of Al alloys", J. Electrochem. Soc., 127, 1325-1331, (1980).

39. H.Kaesche, in Localized Corrosion, Eds., R.W.Staehle et al., NACE, Houston, (1974).

40. T.R.Beck, "Size distribution of etch pits in aluminium", Electrochim. Acta, 33, 1321, (1988).

41. C.Monticelli, G.Brunoro, A.Frignani and F. Zucchi, "Surface-active substances as inhibitors of localized corrosion of the aluminium alloy AA6351", Corr. Sci., 32, 693, (1991).

42. S.L.Chawla and R.K.Gupta, "Materials selection for corrosion control", ASM International, OH, USA, 248, 260, (1993).

43. D.Tomashov and P.Chernova, "Passivity and protection of metals against corrosion", Plenum Press, New York, USA, 67, 70, (1967).

44. G.Tammann, Metal Science, Moscow, ONTI (1935).

45. V.V.Skorchelletti and A.I.Shultin, "Chemical deterioration of metals", Moscow, ONTI, (1938).

46 N.N. Gratsianskii, Doctoral dissertation, Moscow Institute of Physical Chemistry, Akad, Nauk SSSR (1961).

47. A.M.Sukhotin and E.I. Antonovskaya, Zh.Fiz.Khim, 31(7), 1521, (1957).

48. L.M.Kafeli, Dissertation, Moscow (1955).

49. H.H.Uhlig, Z. Electrochem., 62, 700, (1958).

50 P.F.King and H.H.Uhlig, "Passivity in the iron-chromium binary alloys", J. Phys. Chem., 63, 2026-2032 (1959).

51. H.G.Feller and H.H.Uhlig, J. Electrochem. Soc., 107, 864, (1960).

52. A.P.Bond and H.H.Uhlig, J. Electrochem. Soc., 107, 488, (1960).

53. J.Osterwald and H.H.Uhlig, "Anodic polarization and passivity of Ni and Ni-Cu alloys in sulfuric acid", J. Electrochem. Soc., 108, 515-519 (1961).

54. H.H.Uhlig, The Corrosion Handbook, New York, (1948).

MME-1995-M-AKH-COR